PHENIX

Response to Forward Silicon Vertex Tracker (FVTX) Review of 9-July-2007

8 October 2007

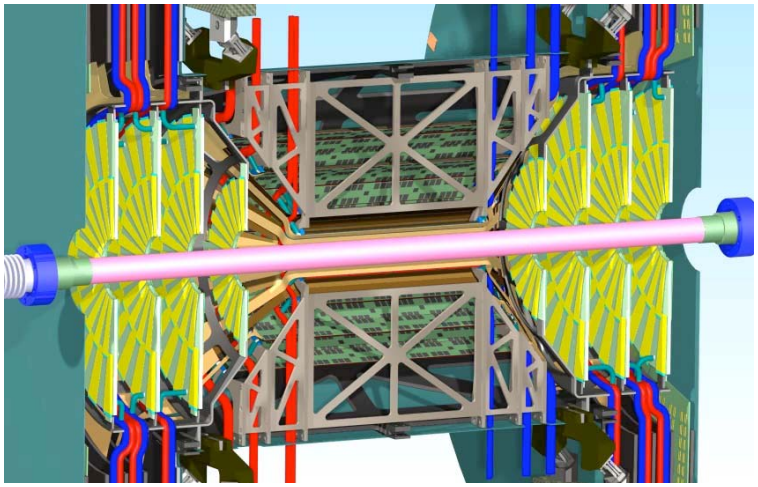

List of Figures

List of Tables

1 Introduction

This write-up is in response to the DOE Scientific review of the FVTX on July 9-10, 2007. We address in this document recommendation I from the review report:

I. *Each detector group should demonstrate and document scientific feasibility for two or more topics of high importance and submit to DOE for evaluation. PHENIX should submit to DOE a report documenting these studies for evaluation, prior to a technical review.*

1.1 Physics Signatures and Backgrounds

a) Heavy Flavor Measurements

The main goal of the RHIC heavy ion program is the discovery and study of the properties of the novel ultra-hot high-density state of matter predicted by the fundamental theory of strong interactions and created in collisions of heavy nuclei, the Quark-Gluon Plasma (QGP). Current results from single non-photonic electron suppression and flow suggest that the heavy quark quenching and thermalization and flow are very large and present the biggest puzzle so far to heavy ion theory [1]. An explosion of theoretical activity in the past couple of years has aimed at understanding the interaction mechanisms of heavy quarks with the plasma [2,3,4]. Advances have been made in understanding the collisional component to parton energy loss in addition to the radiative one. Moreover, novel heavy flavor suppression mechanisms based on heavy flavor dissociation in the QGP have been proposed and shown to be very successful in describing the quenching of the non-photonic electrons. Arguments have also been made that insight from string theory might be useful in understanding the properties of strongly coupled systems. It is widely recognized in the theoretical and experimental communities that progress in this area requires direct measurements of the charm and beauty meson quenching and flow with good precision. With the baseline PHENIX detector, these questions cannot be addressed because the heavy flavor measurements have very large systematic errors due to large backgrounds and there is no capability for separating charm and bottom; therefore, the various model predictions cannot be separated from each other. The FVTX detector will provide precisely this experimental capability to answer the call of the theoretical and experimental communities: provide the definitive determination of the heavy flavor modification mechanism in the QGP and quantitatively pinpoint its properties. The FVTX will allow tagging the parent of single muons at rapidities $1.2 < |y| < 2.4$. This capability will greatly improve the statistical and kinematic reach of the central rapidity measurement using the VTX and electrons in the PHENIX central arms (covering $|y| < .35$). Measuring the rapidity dependence of heavy flavor production will be critical for disentangling cold-nuclear matter effects from QGP effects, and for extrapolating open heavy flavor measurements to predicted recombination charmonium spectra.

The FVTX detector will allow us to make precision heavy flavor measurements by adding the capability to identify particles which have come from a displaced vertex by measuring their distance of closest approach (DCA) to the primary vertex. This DCA will typically be non-zero for secondary particles, as illustrated in Figure 1, and we will use this to tag muons from B and D decays.

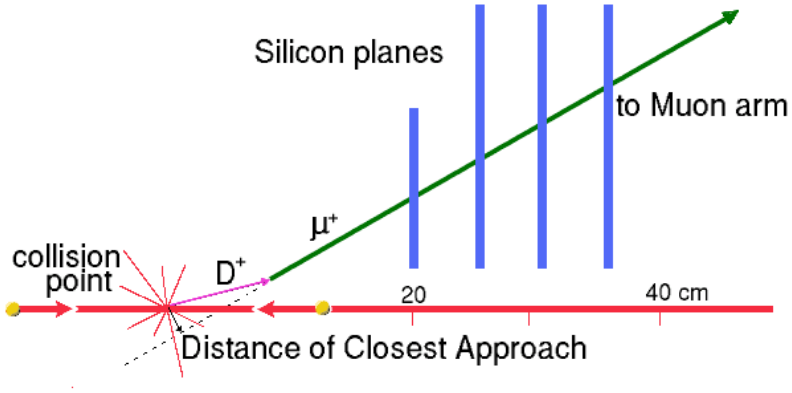

Figure 1 Schematic of the distance of closest approach (DCA) measurement for a secondary particle produced in front of the FVTX detector.

The single particle spectra that are accepted by the muon spectrometers, measured using real data, are shown in Figure 2. Currently, the hadron backgrounds dominate over the heavy flavor components. The hadron backgrounds are comprised of pions and kaons that decay to muons before the absorber material, and those that punch through the absorber material (and may or may not decay in the muon tracker volume). In this report, we present the results of simulations we have carried out to establish the effectiveness of rejecting these backgrounds with the addition of the FVTX detector.

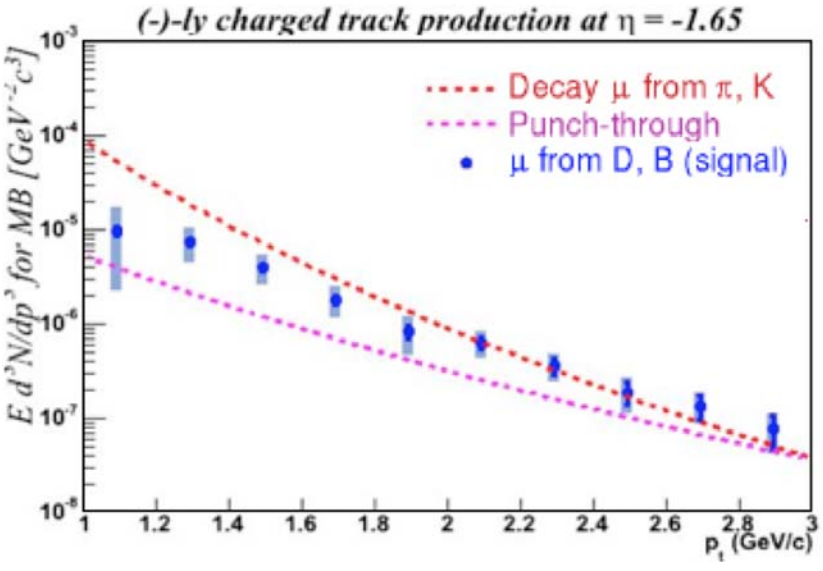

Figure 2 Invariant cross section for heavy flavor muons (blue), hadron decay muons (red) and hadron punch-throughs (pink) contributing to the single particle spectra in the muon arms. Data are derived from real data measurements at RHIC, using the PHENIX muon arms.

b) Vector Meson Measurements

We also present the results of simulation performance studies for ψ' production measurements in heavy-ion collisions. Charmonium and bottomonium bound states offer very sensitive probes of the quark gluon plasma. Survival of the charmonium bound states is expected to be suppressed because the c and cbar pair are screened from each other by the high density of quarks and gluons in the plasma and cannot form a bound state (the color equivalent of Debye screening). The survival probability of the different bound states depends on the binding strength, i.e. the size of the bound system, and the amount of color screening (which is quantified by a "screening length" in plasma physics). Production of bound charmonia is, however, a complicated process that is potentially modified at several stages in the collision. The production rate of heavy quark-antiquark pairs can be modified in Au+Au collisions, with respect to p+p, by changes in the gluon distribution functions of nucleons bound in a nucleus and by initial state energy loss of the gluons. Gluon-gluon fusion is a primary production mechanism for heavy quark anti-quark pairs, so modified gluon distribution functions modify the number and distribution of pairs produced. Energy loss of heavy quarks in the medium will modify the distribution of bound states that are produced. Furthermore, additional contributions to the production from final state recombination when the colliding system cools through the hadronization phase transition can *enhance* production. This is particularly true for charm, if the charm density is high enough. These processes must be measured in order to quantify the suppression due to the Debye screening mentioned above. Adding precision open heavy flavor measurements to PHENIX will help us understand the contribution that comes from recombination as well as initial state effects which are expected be shared between open and closed charm production. To help sort out the magnitude of Debye-screening, we must supplement J/ψ suppression measurements with data on the suppression pattern for vector mesons of different radii, which should be suppressed at different levels. Since the ψ' radius is 0.56 fm compared to the J/ψ which is 0.29 fm, there should be a measurably larger suppression of ψ' than J/ψ if Debye screening contributes to a portion of the measured J/ψ suppression.

We describe below how the FVTX detector will allow the capability of separating ψ' events from J/ψ events in the muon arms by improving the mass resolution of dimuons and by suppressing part of the combinatorial background which lies below the peaks.

1.2 Data Analysis Steps for Physics Extraction

For a heavy flavor analysis, we assume the following analysis steps must be taken for real data. For each, we will note how the analysis step is handled for the FVTX detector in our simulations of physics performance. For all simulations we have also run the full reconstruction chain for the muon arms that is already in use for real data analyses. We

used the PYTHIA event generator for simulating p+p collisions and the HIJING generator for simulationg Au+Au collisions.

- A single muon trigger is implemented online to get a reduced data set which has an enhanced level of events that have at least one particle which penetrates to the deepest layer of the muon identifier system. The same trigger that is currently used in PHENIX is assumed, and the efficiency losses are automatically included in our simulations since our particle spectra are normalized based on real data signal and background counts that have been obtained with this trigger.
- For simulations, we simulate the digitization of Monte Carlo hits into hit strips. For both simulation and real data, cluster finding, track finding (pattern recognition), track matching between the muon tracker (MuTr) and FVTX, and track reconstruction are applied to the data and all reconstructed single particles and their reconstructed track parameters are stored. The DCA, chi-square of the track fit with the FVTX alone and the chi-square for a combined MuTR and FVTX fit are stored to allow for later track selection cuts. For our simulations, we have implemented the full reconstruction analysis for the FVTX system, from cluster formation to track reconstruction, that we would use for real data. We have done this separately for a sample of signal events embedded in HIJING events and for very high statistics (of order four billion events) sets of PYTHIA-generated and single particle generated signals and backgrounds which are not embedded in HIJING events. Efficiency and background corrections were determined from the full multiplicity sample. These corrections are then applied to the high statistics simulation in order to evaluate the physics sensitivity. As the simulation time, especially, but also the reconstruction time are long, it is not feasible to simulate billions of HIJING events. [We note that the multiplicity dependence of reconstruction efficiency and purity in PHENIX real data analyses are evaluated by embedding simulated signals into real Au+Au collision hit data. Of course these do not yet exist for the FVTX detector so we use HIJING generated Au+Au events.]
- Cuts are placed on the reconstructed single particles to reduce background components and thus enhance signal:background for a given signal of interest – in this case, to reduce hadron punch-throughs and hadron decay muons with respect to muons from heavy flavor decay. The same cuts have been applied to the mixed events and to the cleaner PYTHIA events, to understand whether additional corrections should be applied to the PYTHIA event samples to account for lower efficiency for the signal and/or increased background tracks in higher-occupancy events.
- After the above reconstruction steps and single track cuts, the remaining single particle spectra now include heavy flavor muons which dominate over background particles, and not vice versa as is the case without the FVTX. The magnitude of the signal and the remaining background in simulations is calculated as follows: First, the input distributions for punch-through hadrons, decay muons from hadrons, and decay muons from heavy flavor are normalized to the real spectra from each source that have already been measured with the PHENIX muon arms. (Note that we assume that the relative normalization of each

component is the same for Au+Au events and p+p events. Hadrons have been measured to be suppressed in Au+Au collisions with respect to binary scaling, but heavy flavor production also appears to be suppressed at a similar level. Therefore the fractional amounts of each should be similar in Au+Au events and p+p events.) Next, the sum of these components is passed through the reconstruction steps described above. After applying all cuts, we calculate how much of each type of background and how much signal remain. The total signal counts from these simulations are corrected for efficiency losses due to the background rejection cuts and efficiency losses due to imperfect track finding in HIJING events. The background rates are also corrected for any additional background which is created from imperfect track finding in HIJING events and/or reduction in rejection. We then calculate a signal:background ratio and the remaining, accepted signal counts, and from these the statistical and systematic errors for the extracted signal can be calculated (see section 2.6.2).

- The remaining background is handled with the same background subtraction techniques used in analysis of the current muon arm data [5]. The number of muons from π and K decay are determined from the vertex distribution of single particles—more decay muons are produced far from the absorber than close to the absorber so the vertex distribution can be fit to extract the amount of long-lived decay muons contributing to the single particle spectra. The punch-through hadrons are estimated by looking at the distribution of particles that reach each depth of the muon identifier—muons that stop in a given muon identifier layer produce a relatively narrow momentum peak (measured by the muon tracker system) for each layer, but punch-through hadrons populate a long tail in the momentum distribution in a given muon identifier layer since the hadrons interact and lose energy in the material within the muon identifier. Therefore, the momentum distribution at each muon identifier layer can be used to extract a relatively clean sample of punch-throughs that are reaching each layer. The fraction of these hadrons in the total muon sample is extrapolated to beyond the last plane and to higher momenta using Monte Carlo. This procedure is significantly improved with the introduction of the FVTX, since cuts on the FVTX information substantially reduce the background. Significantly smaller statistical errors are incurred in the signal extraction because the background subtracted is smaller. Futhermore, the uncertainty in the normalization of the background contributes less systematic uncertainty in the extracted signal.
- Physics plots are produced based on the number of calculated heavy flavor muons accepted by our cuts, with error bars taking into account the background that must be subtracted (giving an additional statistical error component) and the uncertainty in this background (giving a systematic error component)

For ψ' decaying to dimuon analyses the following analysis steps are assumed:

- A dimuon trigger is implemented online/offline to get a reduced data set which has an enhanced level of dimuons with invariant mass > 2 GeV.

- Track finding and fitting are performed in the muon and FVTX systems. Track matching between the two are performed so that muon track reconstruction can be improved with the addition of FVTX data points to tracks and so additional background rejection can be implemented. For simulations, the ability to match tracks between the FVTX system and the muon system was studied by embedding signal events into HIJING events.
- Cuts are placed on single tracks to reduce the combinatorial background component that comes from hadrons decaying to muons.
- Background dimuons are subtracted from the unlike sign dimuon spectrum using event mixing to determine the background dimuon distribution. The remainder is fit to a dimuon peak plus residual background from heavy flavor and Drell-Yan (which are real unlike-sign backgrounds). The level of background events is based on real Au+Au data. The mass resolution matches the mass resolution observed in real muon arm data with no FVTX. Including the FVTX detector hits into the muon momentum reconstruction narrows the mass resolution, making the extraction of the ψ' peak more accurate.
- Physics plots are made by counting the number of events in the dimuon peak, and correcting for efficiency loss using Monte Carlo simulations to calculate the reconstruction efficiency.

Since we have mature real data analyses of J/ψ signal extraction from AuAu data sets, we know the real performance of the muon system for extracting J/ψs, understand what the background levels are, and have verified that our Monte Carlo models the detector well, so we just need to simulate the additional enhancement that we get from adding the FVTX detector. The enhancement that the FVTX detector provides is to improve the mass resolution of dimuons by accurately measuring the opening angle of the muon pair. The FVTX also enhances background rejection by allowing rejection of hadron decay muons, exactly as we do for the open heavy flavor analyses. It is primarily the enhanced mass resolution which will allow us to separate the ψ' signal from the J/ψ signal in the dimuon mass spectrum.

1.3 Design Specifications for the FVTX

The design specifications for the FVTX are shown in Table 1. They are derived from physics requirements needed to perform the above analyses, electrical, and mechanical requirements.

Integrated Radiation dose	200k rad
Maximum Occupancy per strip	10 %
DCA in r-z plane	<200 μm
Sensor wedge radiation length	< 2.4%
Strip pitch	75 μm
Hits/track	≥ 3
Participation in Level 1 trigger	yes
Azimuthal coverage (phi)	hermetic
Theta coverage	Full muon arm coverage (10-35 deg)

Table 1 Design specifications for the FVTX detector.

The physics requirements are determined from simulations of physics processes of interest using simulations which include the full PHENIX detector geometry. In the simulations it is especially important to include detector components and support structures in the VTX detector as well as ensure that the surrounding detectors and materials are faithfully represented. To accomplish this the FVTX group added to the VTX detector geometry, 1) the HDI flex cables coming from each barrel layer and routed to the outside radius of the barrel, 2) cooling tubes and plenums for the barrel layers, 3) stave support rings for the VTX barrel layers, 4) and the support structures for the stave support rings. The FVTX model was based on the mature mechanical model that we now have in place.

The integrated radiation dose requirement is the expected does that will be delivered in the region of the FVTX detector, for 10 years of RHIC running. Our electronics have been specified to be tolerant of this dosage (an *electronics requirement*). The maximum occupancy requirement is set to 10%, to allow high efficiency track finding, based on our track finding performance measurements and our collective experience with track finding in high occupancy environments. We actually achieve an occupancy of 3% or less in simulations, so retain a factor of 3 contingency so we can handle any unexpected increases in occupancy. The DCA resolution, and corresponding strip pitch is set to allow significant separation of muons from heavy-flavor decay from hadron decay muons and punch-throughs, and has been verified by our detailed simulations which are explained below. The radiation length is specified to be <2.4%, also to maintain our DCA resolution.

2 Simulations

2.1 Event Generation

Single particle spectra: Full PYTHIA events were used to generate heavy flavor decay muons. In total, 120 million D events and 40 million B events were produced and analyzed through the full reconstruction chain as described above, and in more detail below. The spectrum of D and B decay muons produced is shown in Figure 3.

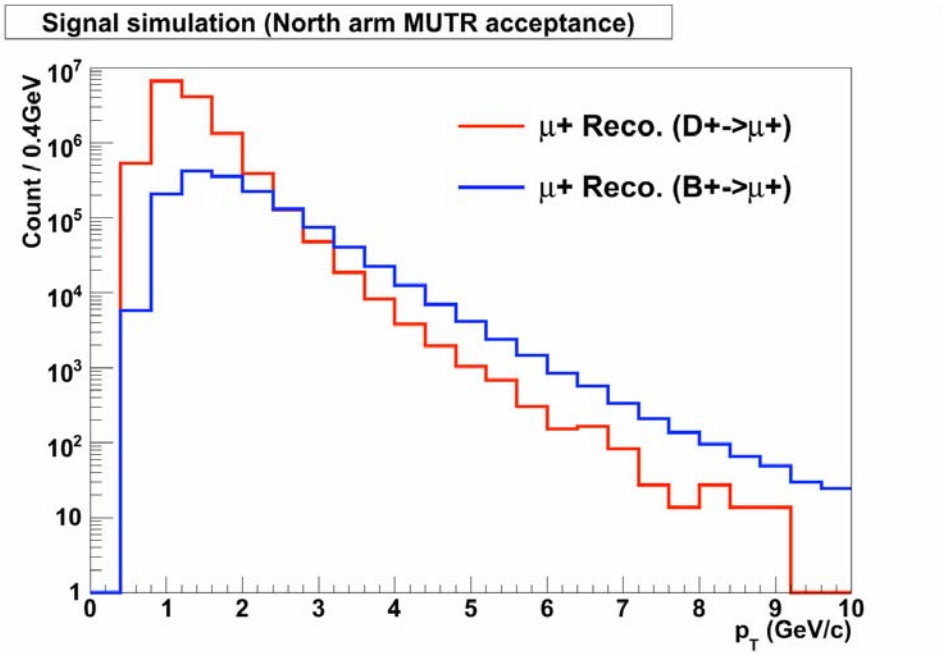

Figure 3 The spectrum of D and B muons that were generated for studying heavy flavor measurements using the FVTX detector.

Backgrounds from π, K were studied using 5 million minimum bias events run through the full reconstruction chain and approximately 4 billion π and K events were simulated to produce sufficient statistical precision for decay muons from π and K along with punch-throughs over the momentum range where we have signal. The large number of hadron events were required to overcome the loss of tracks in the absorber material and to properly populate the moderate- to high-p_T portion of the spectrum with punch-through hadrons, decay muons, as well as hadrons which decay in the muon tracker volume and are mis-reconstructed from lower momenta to higher momenta. In Figure 4 the spectrum of hadrons that were thrown (black solid line), reconstructed in the muon arms (lower solid lines), and the normalized spectra compared to theory, are shown. The relative contributions of muons from hadron decay, punch-through hadrons, and muons from heavy flavor decay to the single particle spectra were ultimately normalized based on real data measurements that were shown in Figure 2.

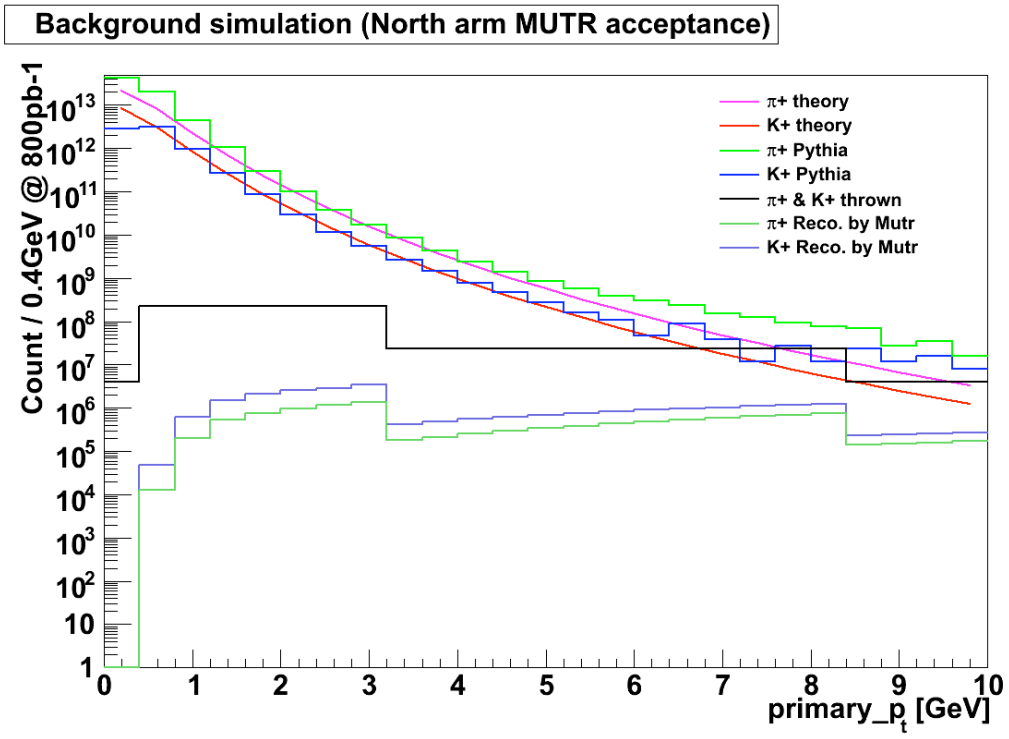

Figure 4 The spectrum of hadrons that were generated (before nomalization) for studying backgrounds for heavy flavor measurements.

Vector Mesons: ψ' events were generated using PYTHIA, and run through our full reconstruction chain to check mass resolution.

2.2 Detector Modeling, Detector Response and Hit Reconstruction

2.2.1 Modeling of the hardware

The detector has been modeled in the GEANT-3-based PHENIX software framework. Since the performance of the device is strongly affected by multiple scattering, great care was taken in representing all materials in the FVTX volume. Tracks reaching the FVTX detector planes typically traverse parts of the VTX; therefore we modeled the VTX barrel support structures, cooling circuits and cables, as well as the new beam pipe, as illustrated in Figure 5.

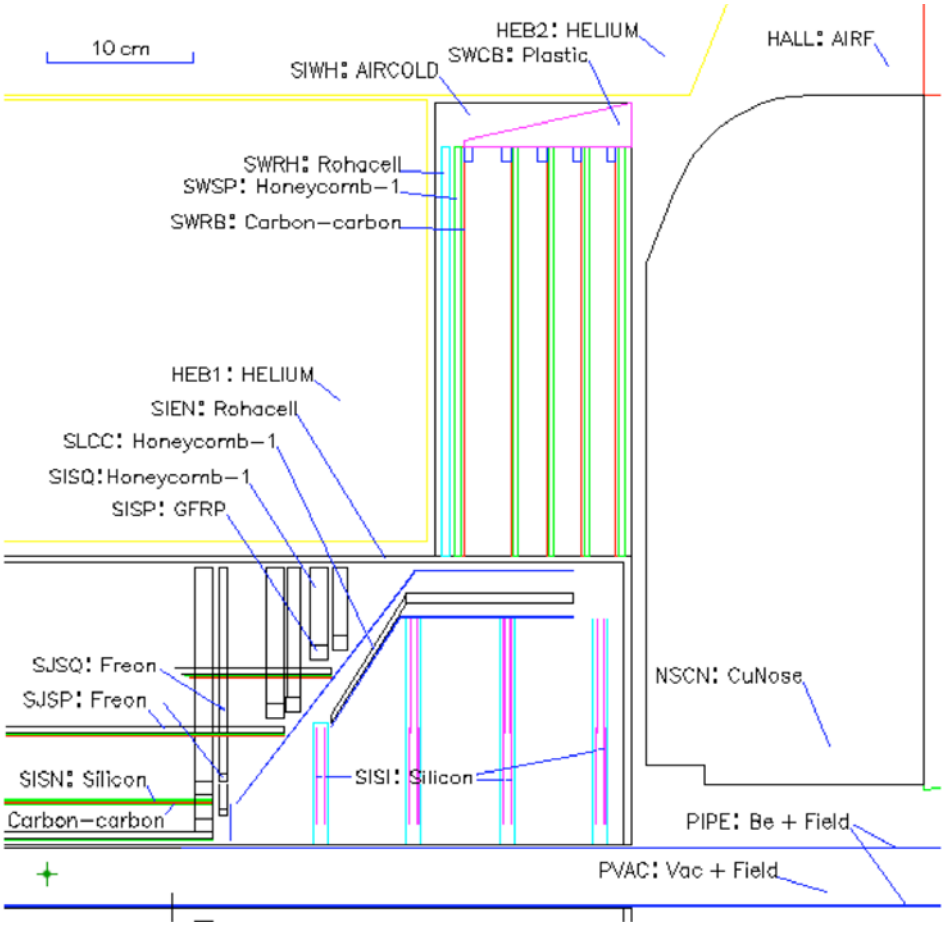

Figure 5 A picture of the simulated FVTX and VTX geometry in our GEANT code.

Additionally, the readout electronics boards, which are located outside the FVTX detector planes, were added to the model. These structures can cause a small amount of 'splashback' tracks into the silicon detector, but more importantly, can cause background tracks for the central arm detectors located at larger radii.

We have run simulations with the current nosecone absorber in place, and with the nosecone calorimeter in place (but without using the active detector elements in our analyses) and verified that the physics performance with the FVTX is nominally the same for both configurations.

All albedo generated from neighboring detectors is naturally included in our simulations.

All simulations used the full and complete modeling of the muon tracker and muon identifier systems.

The real, measured magnetic field was used in all simulations, at both the GEANT stage and the reconstruction stage.

2.2.2 Hit Simulation and Cluster Reconstruction

Tracks typically traverse the silicon planes at angles of 10-30 degrees with respect to the normal. Since the silicon is 300 μm thick, and the silicon is segmented into 75-μm strips, a track typically traverses a cluster of 1-4 adjacent strips. This is illustrated in Figure 6 where the cluster size distribution is shown in the left-hand panel for particles thrown into the acceptance of the FVTX. Including clustering in the simulations is increasingly more important as the occupancy increases, so we have taken care to model the cluster formation in our code. However, even with clustering, our occupancy remains relatively modest. For p-p collisions the probability that hit clusters could overlap from different tracks is exceedingly small because the average number of tracks in each endcap is only about 2.4 (hit occupancy ~.008%). For Au-Au central collisions the hit occupancy can reach ~3% which leads to the probability that 1% of the track clusters will overlap and lead to possible track finding inefficiencies.

In our simulations, the charge deposited in the silicon is shared between strips according to the track length under each strip. A hit location within a cluster is calculated from the mean of the strip locations in a cluster of hit strips. Limited pulse height information for each strip is available, but this is currently not used in the calculation of the hit location though the use of it would improve our hit resolution somewhat. When a cluster is formed by just one strip, the cluster resolution is given by the strip width divided by sqrt(12), or approximately 22 μm. When a cluster is wider than one strip, our resolution improves, even without the pulse height information. This is illustrated in Figure 6 where the resolution of 3-wide clusters is shown and is approximately 10 μm. The resolution is calculated by taking the reconstructed radial position of the cluster minus the true Monte Carlo radial position. It is partially because of the improved resolution that we get from multi-strip clusters that we are able to have strips that are as wide as 75 μm but still retain our desired DCA resolution.

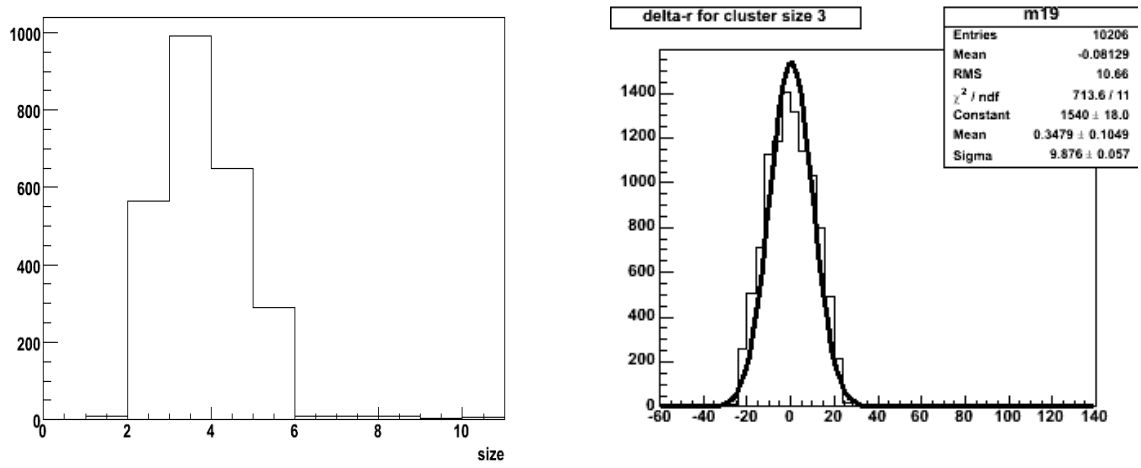

Figure 6 The cluster size for a distribution of particles thrown over the FVTX acceptance (left) and the resolution of the found cluster centroids for 3-wide clusters (approximately 10 μm).

2.3 Track Finding and Reconstruction

2.3.1 Track Finding Algorithm

Once hits (also called coordinates in our nomenclature) have been formed in the silicon system, tracks of interest must be found within a full Au+Au event and fit. Since the occupancy is not so high, the track finding algorithm that we have developed to study our track finding efficiency is a simple algorithm. It is also an algorithm which is still under development, so we expect future improvements in performance, but it already performs reasonably well in the Au+Au environment. The track finding starts tracks with hits in the last station of silicon and looks for additional hits to add to the track in successive forward silicon stations until the silicon station which is closest to the vertex is reached. The window within which hits are searched can be relatively small because of the fine resolution of the detector elements and the relatively small amount of multiple scattering and bending within the magnetic field that the tracks suffer. The windows are nominally $\pm 2^\circ$ in the phi direction (slightly larger than the length of one silicon strip width) and $\pm 0.1^\circ$ in the theta direction (equivalent to approximately ±4 silicon strip widths), with the search windows measured with respect to the nominal vertex (and are wide enough to pick up our finite decay-length signals). A given silicon station is allowed to be skipped, and hits in overlapping volumes within each station are given the opportunity to contribute to the same track.

As a cross-check, a second independent tracking algorithm has also been developed. This algorithm starts with straight-line roads formed by hits in the first and last station, in a selected phi region (currently the width of a silicon strip). Hits are searched in the middle stations and track candidates formed if hits are found in both middle stations

within a residual cut in r. Overlapping hits are automatically included in the search. The first pass imposes a tight cut in r and requires hits on all four stations. Two more passes are performed, widening the windows in each pass and searching only unused hits. The result is that straight-line intermediate and high momentum tracks are found first, with the later passes picking up lower momentum tracks. Currently four-station tracks are reconstructed, but it is straightforward to extend the procedure to tracks intersecting the first three or last three stations. A sample of the results from this algorithm can be seen in Figure 8. We have confirmed that both procedures produce consistent results.

Once candidate tracks are found, they are passed to a Kalman Filter track fitter which swims tracks through the known materials and magnetic field and produces track fit parameters at the nominal vertex. Tracks which are below a given track quality, determined by the fit results and the number of hits, are thrown out. Track matching to the muon system is done only after all FVTX and muon tracks have been separately found.

We also implemented a stage of "ghost track" rejection to reduce the probability of creating incorrect tracks in higher occupancy events. The ghost rejection algorithm compares all tracks which share one or more hits. Of the set of tracks that share one or more hits, the "best" track is selected based on the χ^2 value of the track fit and the total number of coordinates on the track. All tracks but the best track are tagged as a ghost and thrown out of any analysis. This reduces our overall track finding efficiency somewhat (from a nominal 100% to ~95%) but significantly reduces any extra tracks produced in an event so that our signal is not re-contaminated with additional background tracks. All tracks which are kept have DCAs and chi-squares of the fits stored for later track selection.

The efficiency of finding tracks in a full event is defined as:

$$\frac{N_{reconstructed,quality}}{N_{thrown}}$$

Equation 1

where N_{thrown} are the number of Monte Carlo tracks of interest produced which have enough hits in the silicon system to be reconstructed and $N_{reconstructed,\ quality}$ are the number of these tracks, in an embedded event, which are reconstructed, pass reconstruction quality tests (cut on chi-square of the track fit), and have track reconstruction parameters which match the original track. The track reconstruction parameter which is most important to match in the found track is the measured DCA of the track, since the DCA is the primary cut value which is used to separate signal tracks such as heavy flavor muons from background tracks such as muons from hadron decay. For the studies in this report, we have required that all tracks must hit 4 planes of silicon to be reconstructed to allow for the most unambiguous formation of tracks possible. However, we expect that we can regain some efficiency of our signal by later allowing tracks with just three or more planes to be reconstructed, once our algorithms are more finely tuned.

2.3.2 Track Finding Environment

In this section we show a few illustrations of Au+Au events in the FVTX detector to show the track finding environment. Figure 7 shows the strip occupancy that is seen in minimum bias Au+Au events in the forward silicon system. From here, you can see that the occupancies are modest (of order 1.5% or less). Figure 8 shows two side-views of hits in a particular silicon sensor, to illustrate the typical occupancy seen on a sensor. The left-hand panel shows the strip lengths (indicated by vertical lines) that are hit versus the z position. The hits are color coded so common colors belong to hits from a common track. The right-hand panel shows the same hits in the r-z plane, including an inset zoomed picture which indicates that the tracks are reasonably well separated within our detector resolution. Figure 9 shows the hits that occur in some specific silicon sensors in the first station (leaving other sectors out so that the delineation between sectors is clear). Since each sensor has two columns times 680 strips of segmentation, it can be seen that the hit occupancy is small enough for each hit to be clearly separated from other hits.

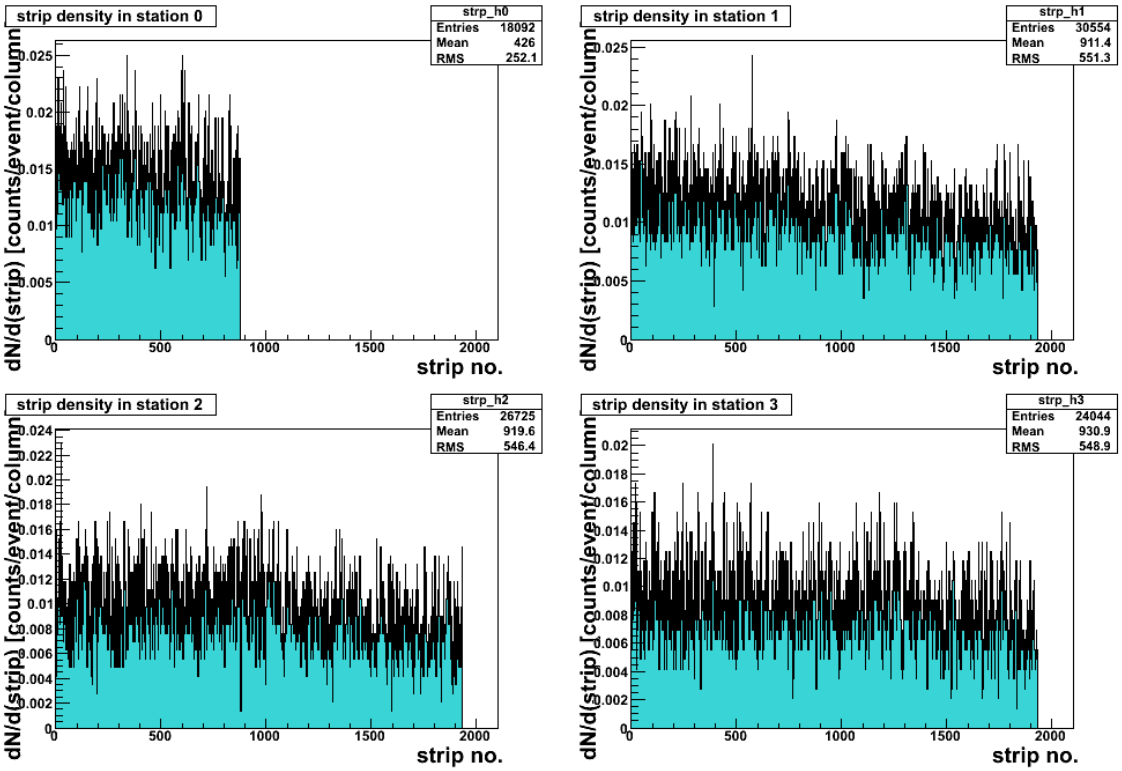

Figure 7 Strip occupancy for each station in the FVTX detector in minimum bias AuAu collisions. The four plots show the occupancies for the four stations

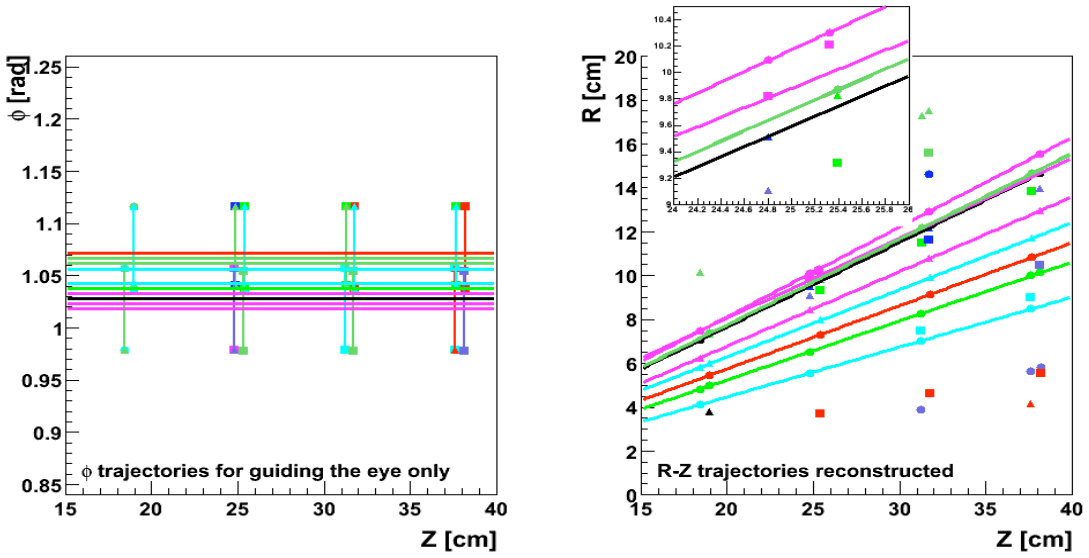

Figure 8 The hit strips in a typical silicon sensor in a minimum bias Au+Au event. Hits from the same MC track are drawn with the same color and marker. The tracks are results of the reconstruction. The left panel shows the hits and tracks in the phi-z projection, and the right panel is the r-z projection. The inset is a zoomed view illustrating the excellent separation of hits on the scale of the detector's segmentation.

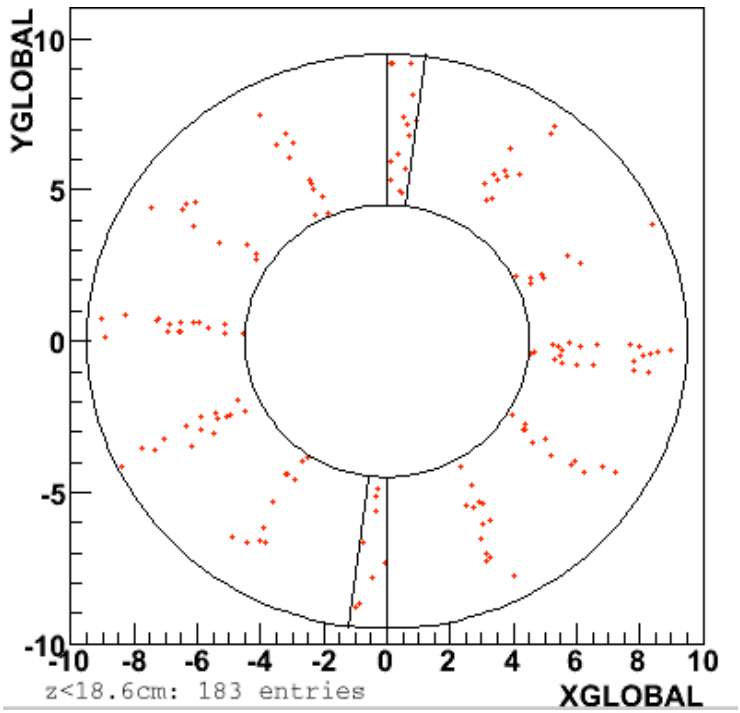

Figure 9 The hits that occur in selected silicon sensors, at station 1, in a central Au+Au event. Two sensors are outlined. Note that each of the sensors has two columns of 640 strips of segmentation to allow separation of the hits.

2.3.3 Track Finding Performance

To study track finding efficiency, we have taken selected signals of interest, embedded them in HIJING events, and counted the number of tracks that are properly reconstructed in the FVTX detector according to Equation 1. We have also looked at the number of additional tracks which are produced which do not contain all the correct track coordinates and are not thrown out with track quality cuts. We refer to these tracks as "ghosts", and they potentially add additional background to our tracks of interest. We have looked at the efficiency and ghosts for single muons from the primary vertex, muons produced by PYTHIA from D and B decay, and hadrons which either punch through the entire muon system or which decay somewhere along the flight path between the vertex and the muon identifier.

Figure 10 shows the efficiency in *unmixed events* that we have with our current algorithm for reconstructing muons from D decay (left) and muons from B decay (right), versus the momentum of the muons. The vertical lines indicate the lower momentum of tracks which can reach the muon system. The tracks above this line are the signal tracks of interest. The average efficiency we get for D decay muons > 2.5 GeV/c is 96% (black points) without a χ^2 cut and 94% (blue points) with a χ^2 cut and the average efficiency for B decay muons is 92% and 91%. Presumably some further tuning of our track finding algorithm would bring the two efficiencies for D and B muons even closer to each other than they already are.

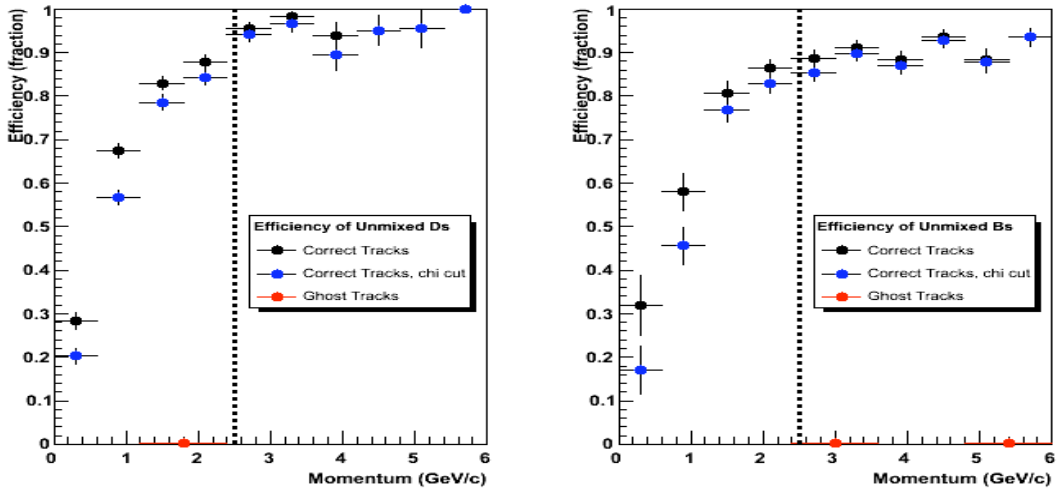

Figure 10 The efficiency for reconstructing muons from D decay (left) and muons from B decay (right), in unmixed events, versus the true momentum. The black points show the efficiency for finding the track (with the majority of hits coming from the true track) and the blue points show the efficiency when an additional χ^2 cut is placed on the tracks.

Figure 11 shows the efficiency for reconstructing muons from D decay when embedded inside a minimum bias AuAu event, with our current software. The left plot shows the efficiency versus momentum and integrated over all centralities. The dashed vertical line indicates again the lower momentum cutoff for muons accepted into the muon system. We maintain very high efficiency for particles which would be reconstructed in the muon arm, with an average efficiency of 94% for muons above 2.5 GeV/c. If a chi-square cut is placed on the reconstructed FVTX track, as we have done in the unmixed analysis, the minimum bias efficiency drops to approximately 89%, and is shown in blue points on the plot. We also show in these plots the fraction of ghosts which are created (red points). This number is maintained at a low level of order 1-2%. The right-hand plot shows the same efficiencies versus detector occupancy, when particles of p>2.5 GeV/c are selected. There is some drop in efficiency as you move to higher occupancy, but the efficiency is still maintained at a reasonably high level. Also note that the occupancy versus centrality is not a linear function so most of Au+Au events are covered by the first two occupancy points that are shown in the figure.

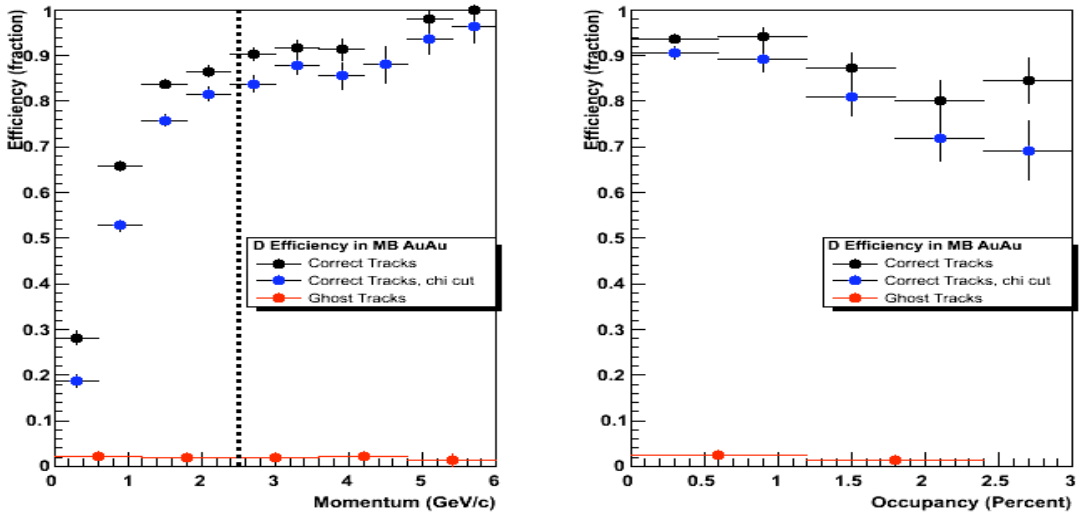

Figure 11 The reconstruction efficiency for muons from D decay in minimum bias AuAu collisions versus momentum (left) and detector occupancy (right). The dashed line on the left shows the approximate lower momentum cutoff for muon arm reconstruction. The red dots indicate the fraction of ghosts that are created.

The same efficiency plots are shown for muons from B decay in Figure 12.

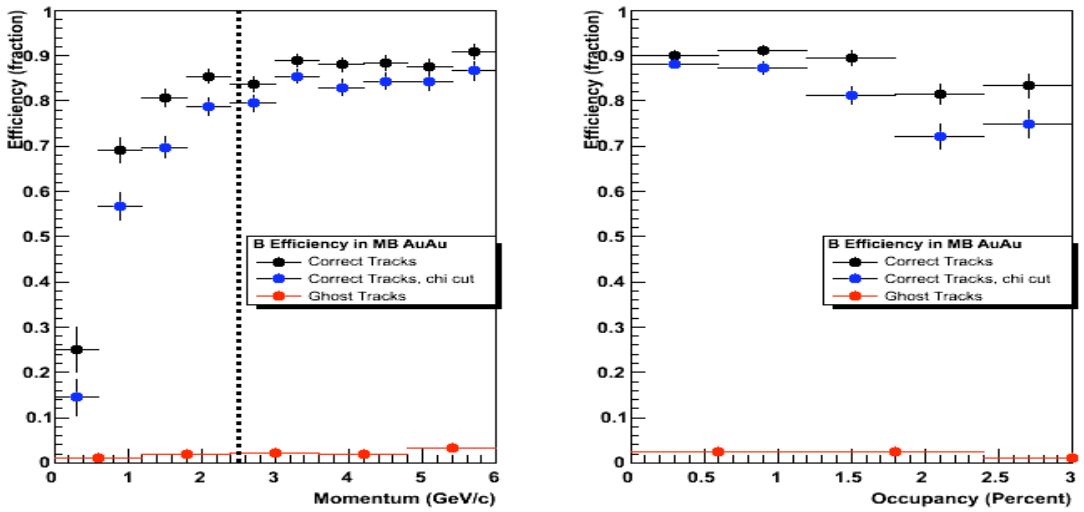

Figure 12 The reconstruction efficiency for muons from B decay embedded in minimum bias AuAu collisions versus momentum (left) and detector occupancy (right. The black dots show the efficiency for finding the track and the blue dots show the efficiency after a χ^2 cut. The red shows the contribution of ghosts to the single particle spectra.

Figure 13 shows the reconstruction efficiency for hadrons. Again, the efficiency is basically the same as it is for the decay muons from heavy flavor decay.

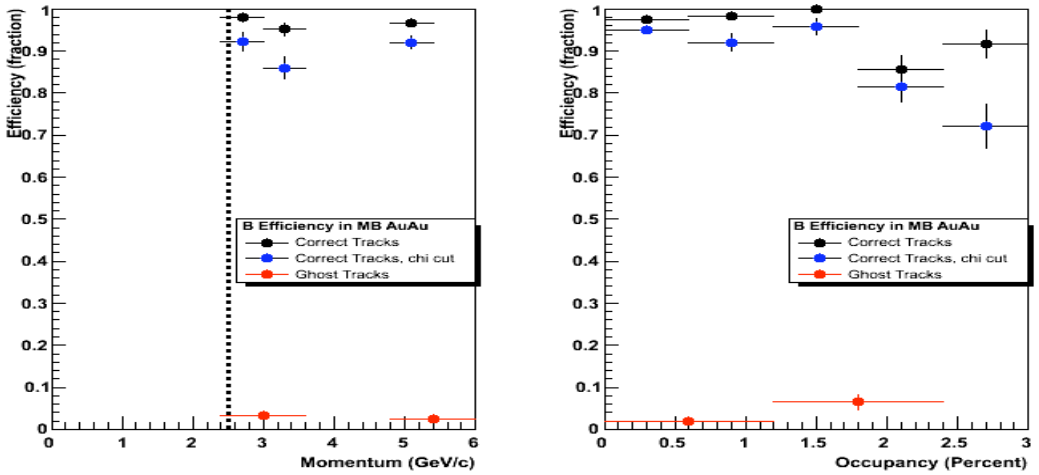

Figure 13 Efficiency for reconstructing pions in minimum bias Au+Au events, versus momentum (left) and detector occupancy (right).

For completeness, we also show in Figure 14 the efficiency for finding tracks, looking at *all* tracks that are created in a Au+Au event, again versus momentum and occupancy.

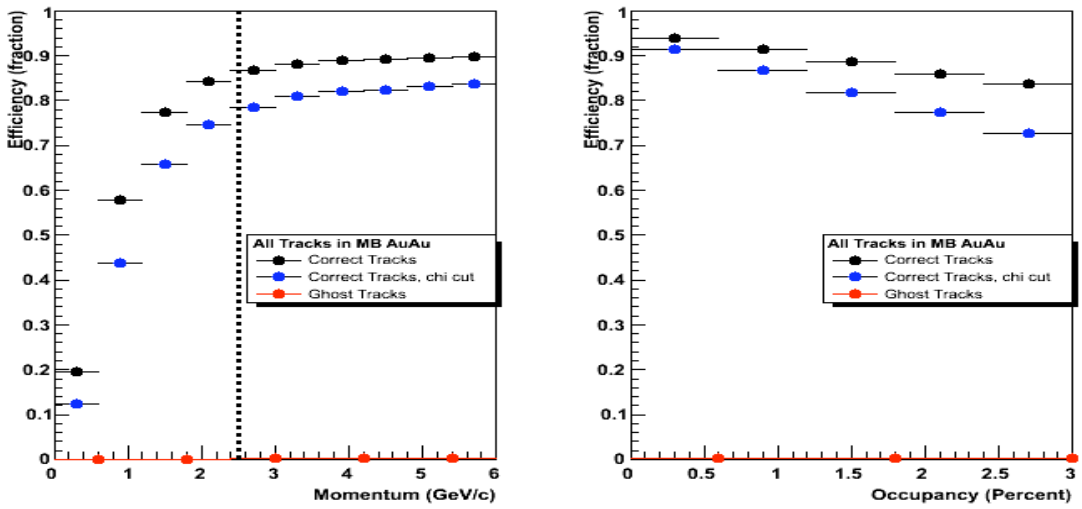

Figure 14 The efficiency for finding all tracks produced in a Au+Au event, versus momentum (left) and detector occupancy (right). The black dots are for finding the track with the majority of the hits correct, and the blue dots are after a χ^2 cut.

Track matching between FVTX and MUTR systems:

Track matching between the FVTX and muon systems is done by taking all reconstructed tracks in the muon system, projecting them forward to the last station of the FVTX system, and gathering any reconstructed FVTX tracks which fall within a search window determined by the muon tracker track. The window is nominally 3 cm radius to allow for scattering in the absorber material between the FVTX and the muon tracker system. All candidate FVTX tracks are fit together with the muon hits from the track of interest and the FVTX track that produces the best combined χ^2 is selected as a correct match. Figure 15 shows the chi-square distributions for correctly matched candidates (red) and incorrectly matched candidates (black) in central Au+Au events.

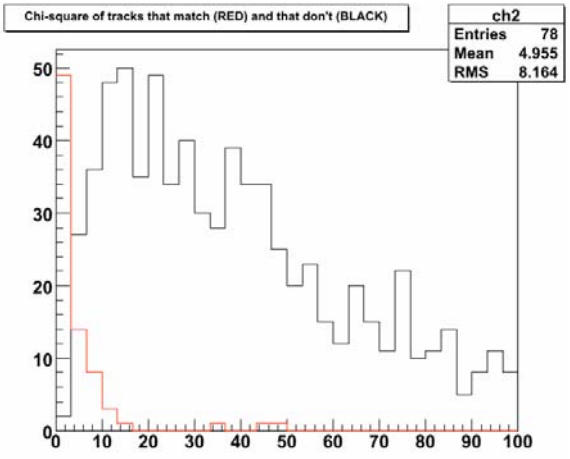

Figure 15 The chi-square distribution for tracks which are correctly matched and fitted between the muon and FVTX systems (red) and ones which are incorrectly matched (black).

The number of tracks which are correctly matched to FVTX tracks, in Au+Au events, is shown in Figure 16. As can be seen, we have reasonably high efficiency for correctly matching the FVTX and MuTr tracks, with an efficiency of approximately 85% achieved over most of the signal region of interest . Even in the central-most high occupancy events we already maintain a reasonably high matching efficiency, and expect this to continue to improve as our algorithms become more advanced.

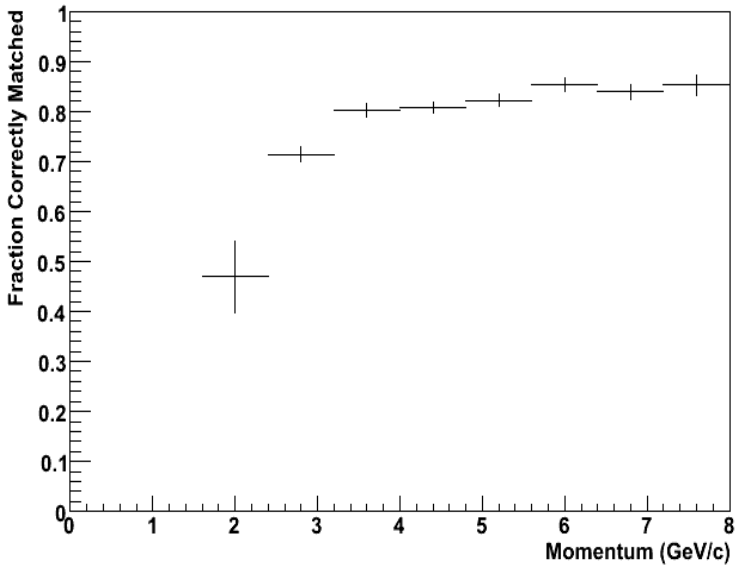

Figure 16 The fraction of reconstructed muon tracks which are correctly matched to an FVTX track versus momentum. Muons from heavy flavor decay were embedded in minimum bias Au+Au events.

2.3.4 Dimuon Mass Reconstruction

The dimuon mass resolution using the muon arm reconstruction is limited by the multiple scattering of the muons in the absorber material in front of the muon system. At the J/ψ mass, the mass resolution has approximately equal contributions to the mass coming from an uncertainty in the total momentum (limited by energy straggling in the absorber) and uncertainty in the opening angle of the muons (limited by the multiple scattering in the absorber). The uncertainty in the opening angle can be significantly reduced by adding the FVTX detector measurement points in front of the absorber material. We have determined the improvement that the FVTX brings to the mass resolution by running J/ψ and ψ' events through the full reconstruction chain and fitting the combined FVTX and MuTr tracks and calculating the dimuon mass from these re-fit tracks. This resolution is then compared them to the muon-fit only resolution. The resulting improvement is shown in Figure 18 for p+p events, and for minimum bias Au+Au events before and after background subtraction since the peaks are difficult to see with AuAu background. The background levels without the FVTX detector are based on real data measurements taken using the muon arms.

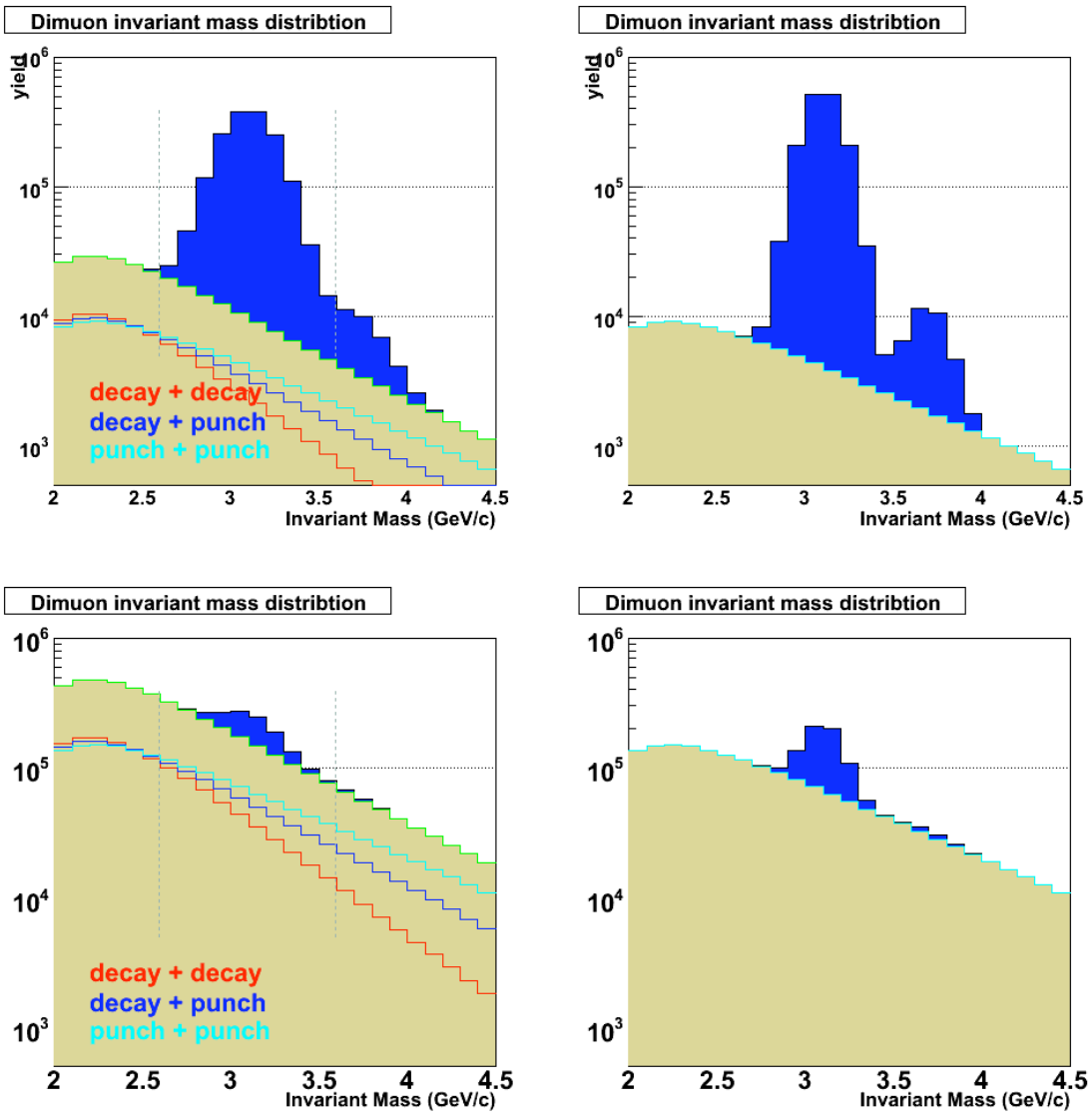

Figure 17 Dimuon mass spectrum for p+p (top frames) and minimum bias Au+Au (bottom frames) events, with (right) and without (left) the FVTX detector. Clear improvements inthe mass resolution and combinatorial background rejection can be seen.

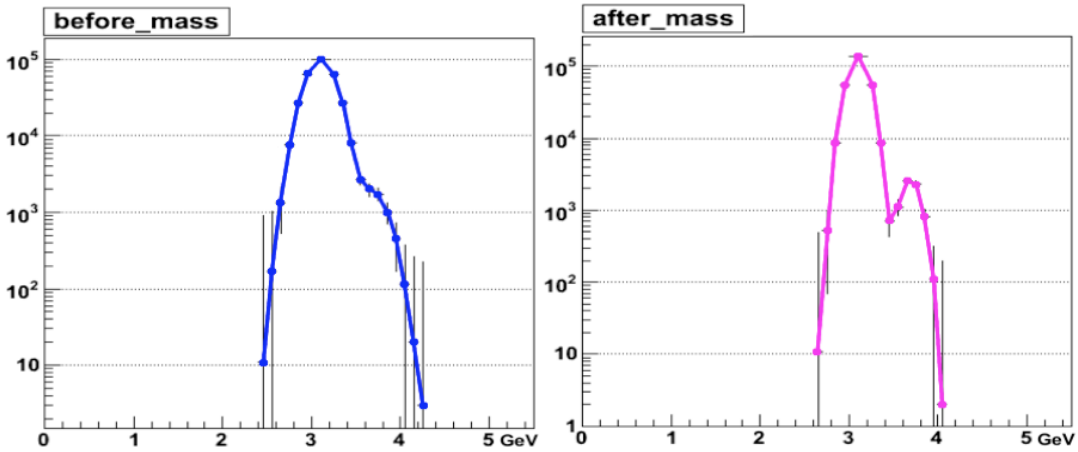

Figure 18 The dimuon mass resolution and signal:background before and after the FVTX detector is used, for minimum bias AuAu events, with background subtracted.

2.4 Event vertex reconstruction.

Preliminary knowledge of the event vertex is an important ingredient in later track finding and reconstruction. Although a rough estimate of the vertex position is available from the Beam-Beam Counter (BBC), this has a resolution of only a couple cm. The barrel Silicon detector (VTX) will determine the vertex with good resolution, of order <100 μm, but we can derive the event vertex from data in the FVTX itself or in conjunction with the VTX detector. This allows the possibility of doing reconstruction with the FVTX alone, and also allows the FVTX to contribute to the vertex finding and resolution, which may be important especially in low occupancy p+p events.

The vertex finding algorithm makes use of the fact that charged-particle tracks in the forward direction are deflected very little by the magnetic field, and therefore hits in the four endcap layers are roughly aligned. Assuming that the vertex lies on the z-axis, one selects a trial z-position for the vertex, and plots for each hit on each plane the angle theta with respect to the z-axis (Figure 19-a). If the trial vertex is not near the real vertex, hits will not line up, and the mean number of entries in these incorrect vertex bins will be a little more than 1. If the trial vertex is in the real vertex location, hits will line up and the mean number of entries in the real vertex bin will be a little under 3. Figure 19 shows this mean for trial vertices between -10 and +10 cm. The location of the highest bin corresponds to the real vertex location.

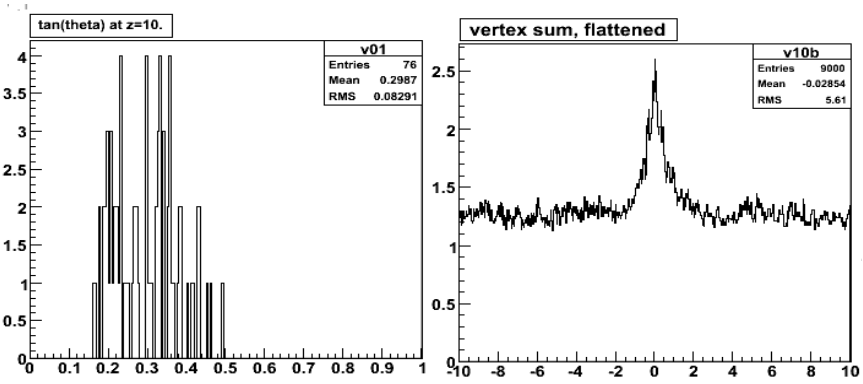

Figure 19 Plots illustrating the vertex-finding algorithm: panel (a) an example theta distribution for a candidate vertex point (b) the number of entries found for different candidate vertices.

2.5 Luminosity assumptions

For the plots generated in this document, we have assumed one year running at either RHIC I or RHIC II luminosities, as designated in text. For RHIC I luminosities, we have assumed 2 nb^{-2} delivered luminosity for one year of Au+Au running, and 70 pb-1 for one

year of p+p running. For RHIC II we have assumed 396 pb^{-1} for one year of p+p running. We have also included luminosity reduction factors to our statistics when producing physics plots. These factors are:

- 55% for |z vertex| < 10 cm
- 60% PHENIX duty factor
- 79% min-bias p+p trigger efficiency, 90% for Au+Au trigger efficiency
- 90% trigger efficiency
- 90% for p+p reconstruction efficiency, 70% for Au+Au efficiency

Multiplying these together gives, for instance, the equivalent of 14 pb^{-1} for one year of p+p for RHIC I and 83 pb^{-1} for one year of p+p for RHIC II. Some double-counting of inefficiencies are in place since we also separately correct our simulated data for reconstruction efficiency of the specific signal of interest.

2.6 Putting it All Together

2.6.1 Reconstructed Signals and Backgrounds for Heavy Flavor

To produce expected physics plots, the 4.2 billion events outlined in section 2.1 were run through the full reconstruction chain that has been described. To each track, we applied the following cuts:

- MuTr + FVTX track fit χ^2 /ndf < 5
- $DCA_{min} < DCA(r) < DCA_{max}$ (to reject punch-throughs and hadron decay μs)
- $DCA_{min} < DCA(\phi) < DCA_{max}$ (to reject punch-throughs and hadron decay μs)
- Isolation cuts (can only be used in p+p events)

to enhance the signal:background ratio of heavy flavor muons over muons from hadron decay plus punch-through hadrons. The DCA cuts are p_T dependent since the resolution and typical DCA for particles changes with p_T. The DCA(ϕ) cuts nominally require that the absolute value of the DCA be less than approximately 500 μm. This cut primarily reduces the hadron decay component. The DCA(r) cut nominally requires that the DCA be greater than -1.0 mm and less than something that is close to zero (p_T-dependent). This cut further reduces the hadron decay component of the background as well as the hadron punch-through component. The full MuTr+FVTX track fit χ^2 cut reduces, especially, the background component from hadrons which decay or interact along the track trajectory.

The relative normalization of the thrown signals and backgrounds was determined from Figure 2. Using this normalization on our thrown events, and the cuts described above, we produce the signal:background ratios before and after cuts, for D^+, D^-, B^+ and B^- in Figure 20 and Figure 21. As can be seen, we get roughly an order of magnitude improvement in the signal:background ratio in all cases, and we make the critical improvement in almost all cases of moving from a signal:background which is less than one to a ratio that is greater than one. It is in this regime of signal:background ratio

changes where the most significant improvements in the error bars in signal extraction can be made, as is shown in section 2.6.2.

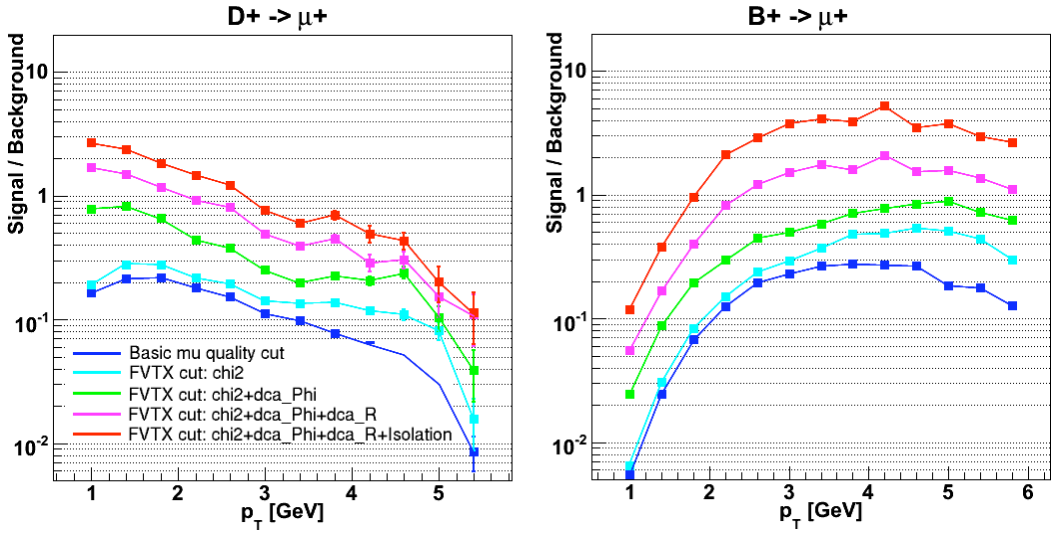

Figure 20 – Signal to background improvement for Ds (left) and Bs (right) which decay to μ^+ for no FVTX cuts and successive FVTX cuts. Cuts applied are χ^2 cut, DCA cut in the phi direction, and DCA cut in the r direction.

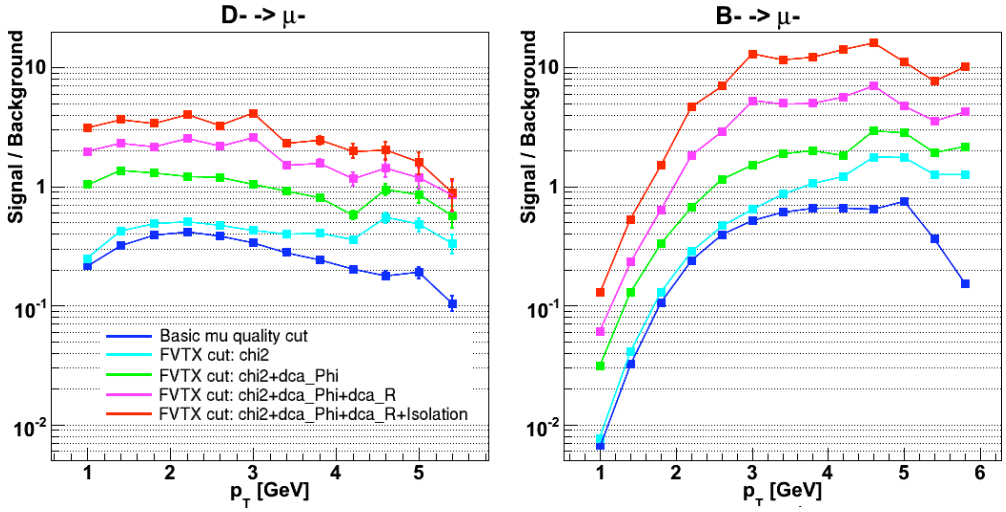

Figure 21 - Signal to background improvement for Ds (left) and Bs (right) which decay to μ^- for no FVTX cuts and successive FVTX cuts. Cuts applied are χ^2 cut, DCA cut in the phi direction, and DCA cut in the r direction.

Corrections to the signal and background are made based on the efficiencies we determined in section 2.3. The signal:background ratio measured above is recalculated to be:

$$\frac{signal * (eff\_sig\_HIJING / eff\_sig\_unmix)}{background * (eff\_bkd\_HIJING) / (eff\_bkd\_unmix) * (1 + ghosts)} \qquad \textbf{(Equation 2)}$$

where eff_sig_HIJING/eff_sig_unmix is the ratio of the reconstruction efficiency in HIJING events divided by the reconstruction efficiency in unmixed events, and the ghosts are all allotted to the background to be conservative (this is likely an overestimate of the increase in background tracks). Since the efficiency for signal and background tracks has been found to be approximately the same, the signal:background ratio does not change significantly because of track finding efficiency. The main change moving from p+p events to Au+Au events is to reduce the overall signal counts by (1) the reduced track finding efficiency and (2) by incorrectly matching a signal track in the muon system to a background track in the FVTX system (overall reduction is approximately 0.8 of p+p). In addition, the background levels are increased slightly because of the ghost tracks and because mis-matching of tracks between the muon system and the FVTX system. Both of these are rather small effects because the number of ghost tracks we form is small and because most of the mis-matched muon tracks will still be thrown out by background cuts.

2.6.2 Statistical and Systematic Error Bar Calculations

The statistical and systematic error bars for a heavy flavor measurement using single particle spectra can be calculated from the signal:background ratios that we obtained above.

The statistical error will improve as the signal:background improves because less background needs to be subtracted to obtain the signal. This is indicated in the following equations where the error in the signal (S) is given with respect to the fraction (f) of the total counts which are background (B) counts, i.e. f = B/(S+B).

$$
\begin{aligned}
&S = N - B; \\
&\delta S = \sqrt{\delta^2 N + \delta^2 B} = \sqrt{\delta^2 N + f^2 \delta^2 N}; \\
&here, \delta N = \sqrt{N}; \\
&N = S + B = S + fN \Rightarrow N = \frac{S}{1-f}; \\
&\delta S = \sqrt{\frac{S}{1-f}(1+f^2)} = \sqrt{S}\sqrt{\frac{1+f^2}{1-f}}
\end{aligned}
$$

Equation 3

As seen, the statistical error will become smaller as the fraction (f), that is background, is reduced.

The systematic errors also improve because the uncertainty in the background normalization contributes less to the systematic error as the background gets reduced. This is indicated in the following equations where the systematic error is given as a

function of the uncertainty of the fraction (f) of the counts which are background. As f becomes smaller, the contribution of δf/f to the systematic error also becomes smaller.

$$\delta S_{sys} = \delta B_{sys} = \sqrt{N^2 \delta^2 f} = N\delta f$$
$$= \frac{s}{1-f}\delta f = s(\frac{1}{1-f})\delta f = s(\frac{f}{1-f})(\frac{\delta f}{f});$$

Equation 4

A plot of the error bars versus the signal:background (see Figure 22, for example, where the systematic error is plotted vs. signal:background) reveals that the largest change in the error bars is made in the region where the signal:background changes from less than about 0.5 to greater than 0.5 which is why, you will see, we obtain a large improvement in our error bars with our signal:background improvement.

$$k(SB) := \frac{\frac{1}{SB+1}}{1-\frac{1}{SB+1}}$$

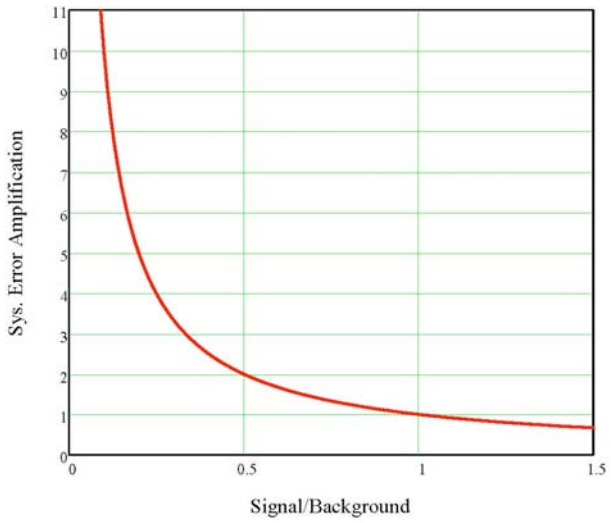

Figure 22 The systematic error associated with a heavy flavor measurement, as a function of the signal:background ratio.

2.7 Physics Measurements

2.7.1 Heavy Flavor R_{AA}

Using the above simulations through to error bar calculations, we produce the simulated heavy flavor cross section plot, with error bars, shown in Figure 23. One year of RHIC I luminosity is assumed. The red error bars indicate the measurement capabilities of the muon system alone and the blue error bars are the error bars we obtain with the FVTX system. As can be seen, with the FVTX system we move from qualitative measurements of heavy flavor production because of the large error bars, to quantitative measurements which allow for precision measurements of the differential cross section.

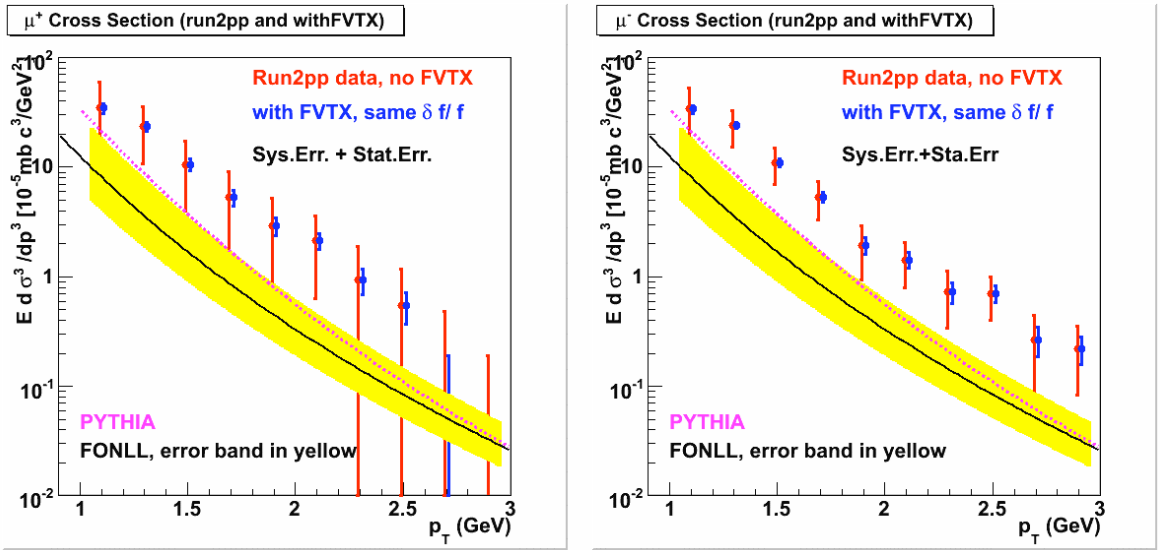

Figure 23 The measurement capabilities of the Muon System with (blue points) and without (red points) are shown for a heavy flavor cross section measurement versus p_T.

Figure 24 shows the R_{AA} measurement capabilities with the FVTX detector, calculated by determining the statistical and systematic error bars for both p+p and Au+Au data sets, combining the error bars appropriately for the ratio, and including all the higher occupancy corrections required in the error calculations. In this figure, the R_{AA} measurement we can attain, versus p_T, is shown for one Au+Au run at RHIC I luminosities, compared to three model predictions for combined charm+beauty suppression [6,3,2]. We show our data points on top of two of the models, to show comparison of two possible outcomes of our measurement. The theoretical model that produced the green band includes just radiative energy loss, and is a model which produces light quark suppressions which are consistent with real data measurements. The blue band adds elastic scattering energy loss to the model. The yellow band includes radiative energy loss plus dissociative energy loss (the mesons lose energy by dissociating, scattering and losing energy, and re-associating into a meson but at lower momentum). As can be seen by this figure, our heavy flavor measurement capabilities will allow us to very clearly distinguish among the different energy loss models. By discriminating among the different models we can determine whether radiative energy loss alone can describe light and heavy quark suppression in heavy ion collisions (green band), and if not, whether elastic scattering or dissociative energy loss are the source of any additional suppression in the heavy quark sector. If dissociative energy loss, which has the unique feature that the suppression remains large for

both charm and beauty (and the sum of the two) over a large p_T range, fits the data best then we will have access to additional information about the formation time of the plasma through the suppression measurement of heavy flavor mesons. Because the mesons are most suppressed when they have formed when the plasma is most dense, the shape of the p_T spectrum is sensitive to the plasma formation time. This is illustrated in Figure 25 where the R_{AA} predictions for heavy flavor or shown versus p_T for two different plasma formation times [7].

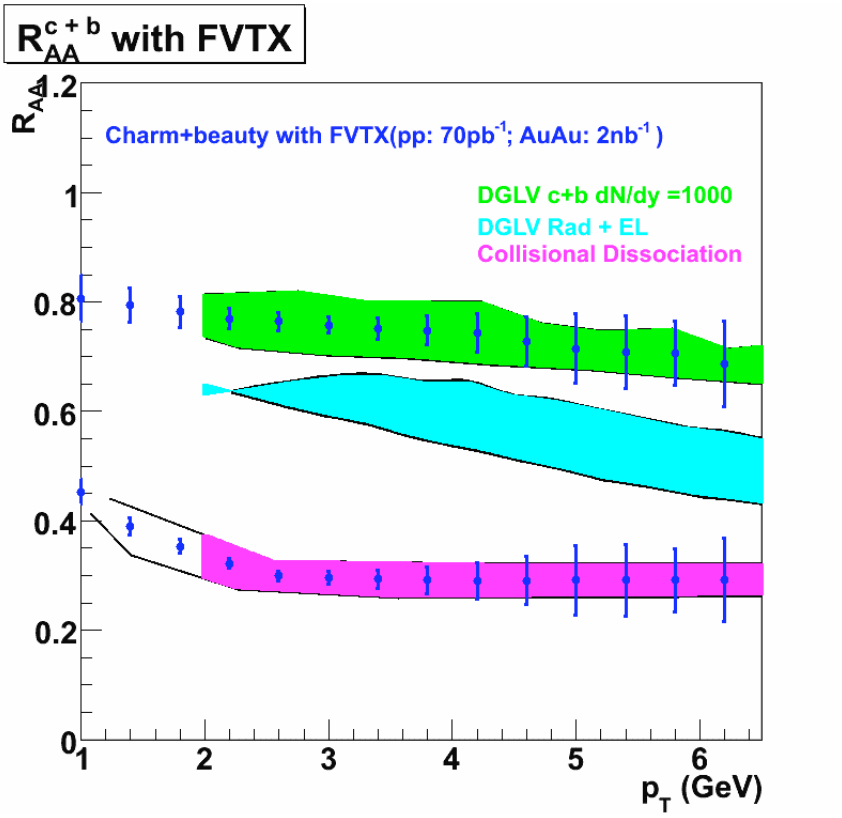

Figure 24 R_{AA} measurement capabilities with the FVTX detector are shown for an inclusive charm plus beauty measurement at $1.2 < |y| < 2.4$, versus p_T. The measurements are shown as blue data points for two possible outcomes, based on two theoretical predictions. Three different model predictions are shown which include radiative energy loss (green), radiative and elastic scattering energy loss (blue) and radiative plus dissociative energy loss (yellow).

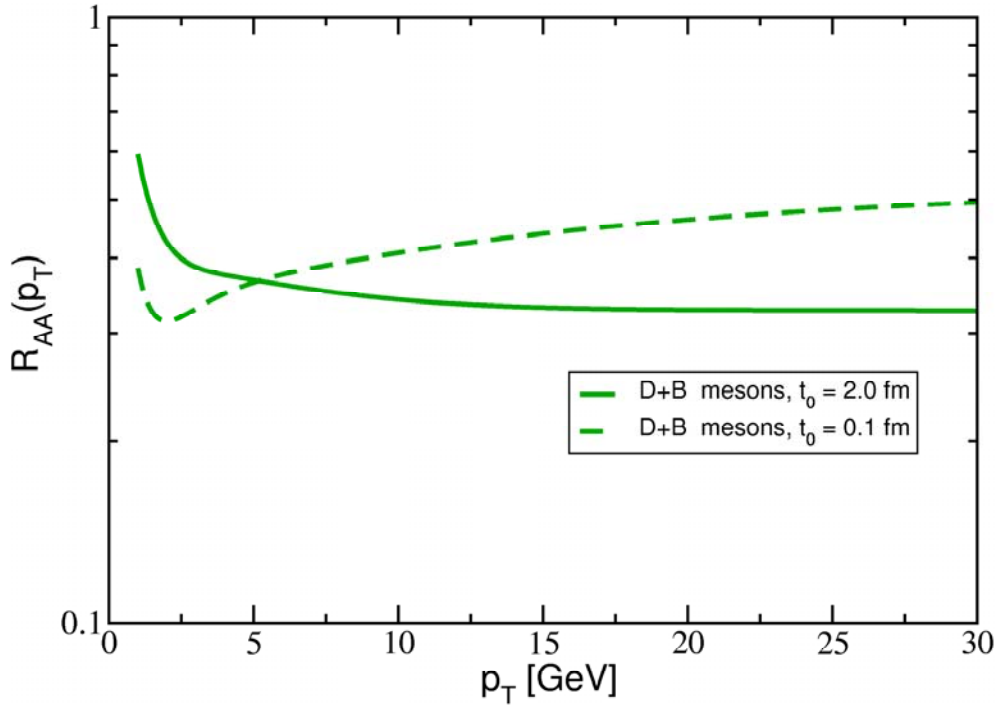

Figure 25 R_{AA} of D+B versus p_T for two different plasma formation times: 2.0 fm and 0.1 fm, in the radiative plus dissociative energy loss model.

Separation of Charm and Beauty

We can potentially get even more information if we separate the charm and beauty components in our R_{AA} measurement since the relative suppressions of charm and beauty are different for the different models. The best separation will likely be achieved through a statistical analysis of our spectra, and this can be achieved in a few ways. (1) Since the lifetimes for charm and beauty are different, and known, the suppression pattern can be measured as a function of a cut on the DCA. The two unknowns (charm suppression factor and beauty suppression factor) can be extracted from a fit to the suppression function versus a cut on the DCA, extracted at several values of p_T. (2) The beauty suppression pattern will be measured directly in the muon arms using $B \rightarrow J/\psi$. With this measurement, we can pull out the beauty component and look at the remaining charm suppression. In addition to this, we have some capability with the FVTX detector to tag charm and beauty events on an event-by-event basis. Since the muons from B decay tend to have a higher p_T with respect to the parent meson than muons from D decay, have a larger DCA, and have different average particle multiplicity associated with them, we can use these event topology cuts to favor muons from D mesons over B mesons and vice versa. An example of this type of measurement is shown in Figure 26 where we have made a cut on the muon p_T to favor charm or beauty and plotted the resulting charm (left) and beauty (right) measurements separately. Again, we show comparison to two different model calculations and plot our data points on top of both of the predictions. The blue is a prediction for

radiative plus elastic scattering energy loss and the green is for radiative plus dissociative energy loss. We lose statistics in this type of measurement, but at low to moderate p_T, our single muon statistics are rather high so the error bars remain reasonable.

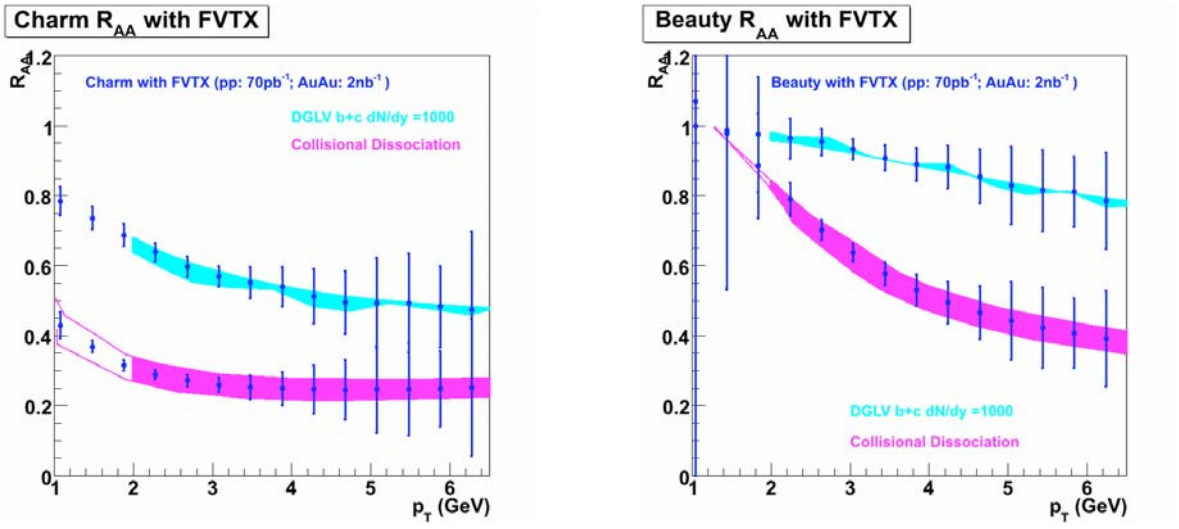

Figure 26 FVTX measurements of charm R_{AA} (left) and beauty (right). Two theory plots are shown for comparison (blue) includes radiative and elastic scattering energy losses and (blue) includes radiative and dissociative energy losses.

2.7.2 Heavy Flavor Asymmetry Measurements

We have also taken our simulated heavy flavor measurements and produced physics plots for a heavy flavor A_{LL} measurement. Heavy flavor measurements in polarized p+p collisions are sensitive to the polarized gluon distribution function since much of the production of heavy flavor is through gluon-gluon fusion. By measuring the heavy flavor production at forward rapidity we are not only sensitive to the polarized gluon distribution function, but we are sensitive in x regions which are not accessible to the central rapidity detectors, therefore allowing PHENIX to have sensitivity to gluon distributions over a much larger x space than is possible with the central detectors alone. Since the central rapidity measurements continue to produce measurements which are consistent with no gluon polarization, these forward rapidity measurements will likely be critical to determining whether there is any gluon contribution to the proton's spin.

The additional x coverage provided by the FVTX is indicated in Figure 27 where the x coverage of different heavy flavor measurements is shown for the FVTX detector (red bars), the current central detectors (blue bars) and the central detectors with the VTX barrel silicon detector (green bars). As can be seen, the FVTX detector significantly expands the x coverage down to small x and up to larger values of x. Note, even though our inclusive

measurements do not allow us to map our measurements on an event-by-event basis directly on to x-space, the theoretical models can easily calculate the expected A_{LL} for a given measurement, as well as its p_T dependence. It is this predicted A_{LL}, compared to our measurements, which will tell us whether our measurements are consistent with one polarized gluon distribution function or another. (Please see Appendix A for more details about extracting physics from our asymmetry measurements.)

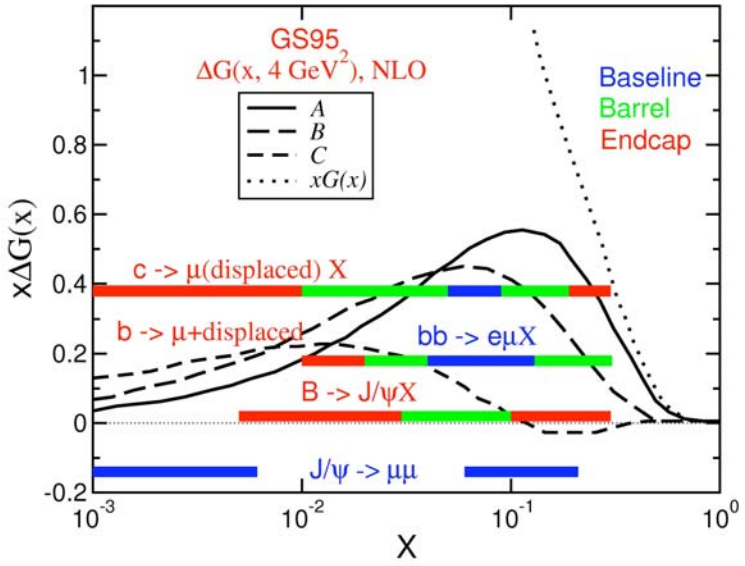

Figure 27 The x coverage of FVTX heavy flavor measurements (red bars), along with Gerhmann-Stirling A, B, C distribution functions.

Experimentally we measure the double spin asymmetry;

$$A_{LL}^{Q\overline{Q}} = \frac{\sigma^{++} - \sigma^{+-}}{\sigma^{++} + \sigma^{+-}} \sim \frac{\Delta G(x_1)}{G(x_1)} \otimes \frac{\Delta G(x_2)}{G(x_2)} a_{LL}(x_1 + x_2 \to Q\overline{Q} + X)$$

Equation 5

The partonic asymmetry $a_{LL}(x_1 + x_2 \to H + X)$ is calculated within the framework of pQCD. In the PHENIX experiment, we will measure the polarized gluon distribution $\frac{\Delta G(x)}{G(x)}$ using many different processes. However, in reality, one always faces various backgrounds in the measurement, so the measured signal asymmetry is diluted, according to the following equations:

$$A_{LL}^{S} = \frac{A_{LL}^{in} - fA_{LL}^{B}}{1-f};$$

$$\delta A_{LL}^{S} = \frac{\delta(A_{LL}^{in} - fA_{LL}^{B})}{1-f} + (-1)\frac{A_{LL}^{in} - fA_{LL}^{B}}{(1-f)^2}\delta(1-f);$$

$$\delta A_{LL}^{S} = \frac{\sqrt{\delta^2 A_{LL}^{in} + f^2\delta^2 A_{LL}^{B})}}{1-f} + (-1)\frac{A_{LL}^{in} - fA_{LL}^{B}}{(1-f)}(-1)\frac{df}{1-f};$$

$$\delta A_{LL}^{S} = \frac{\sqrt{\delta^2 A_{LL}^{in} + f^2\delta^2 A_{LL}^{B})}}{1-f} + \ldots A_{LL}^{B} * \delta f \ldots + A_{LL}^{S}\frac{f}{1-f}\frac{\delta f}{f}; A_{LL}^{B} = 0;$$

Equation 6

where $f = \frac{N^{BG}}{N^{Q\bar{Q}} + N^{BG}}$ is the background fraction, and A_{LL}^{in} and A_{LL}^{B} are the asymmetries of the inclusive signal and background, respectively. From this, you can pull out and calculate the statistical error portion (first term), by making the following substitutions:

$$A_{LL} = \frac{1}{P_b P_y}\frac{N^{++} - RN^{+-}}{N^{++} + RN^{+-}}; A_{LL} \approx \frac{1}{P_b P_y} * \frac{1}{\sqrt{N}};$$

$$statistical: \delta A_{LL} \propto (c = \frac{1}{\sqrt{2P^2}})\frac{\sqrt{1/N + f^2(1/B)}}{1-f} = \frac{1}{\sqrt{S}}\sqrt{\frac{1+f}{1-f}}$$

Equation 7

and the systematic error is equivalent to the last term in Equation 6.

For our A_{LL} error bar calculations, we have used our calculated signal:background ratios to determine the fraction of background we have and have assumed the asymmetry from the remaining hadronic background in our measurements is zero. The beam polarization, needed for calculating the statistical portion of the error, was assumed to be 0.7.

The resulting heavy flavor A_{LL} measurement capability, using single muons, is shown in Figure 28, versus p_T, in this case for RHIC II running and at 200 GeV. The red error bars indicate the measurement capability with the FVTX detector, calculated as outlined above. The theoretical curves are A_{LL} calculations which use LO calculations (NLO calculations are not yet available, but are in process) to get the partonic asymmetry and Gehrmann and Stirling A and C (GS-A, GS-C) polarized gluon distributions, and GRSV-STD and GRSV-MAX distributions. As can be seen from the picture, the heavy flavor A_{LL} measurement will allow us to separate, especially, the GS-C and GRSV-STD from the GS-A and GRSV-Max models. The distinction becomes especially clear at moderate to hight p_T. The inclusive heavy flavor measurement is directly sensitive to the different models, but we can

also get information about the charm and beauty components separately, as we have indicated we would do for the heavy flavor R_{AA} measurements. By calculating the A_{LL} values versus different DCA cuts, we can deconvolute the charm and beauty contributions to our inclusive A_{LL} measurement. The separation of the two primarily improves our sensitivity at low p_T, as indicated in where a beauty-only A_{LL} measurement is indicated in Figure 29.

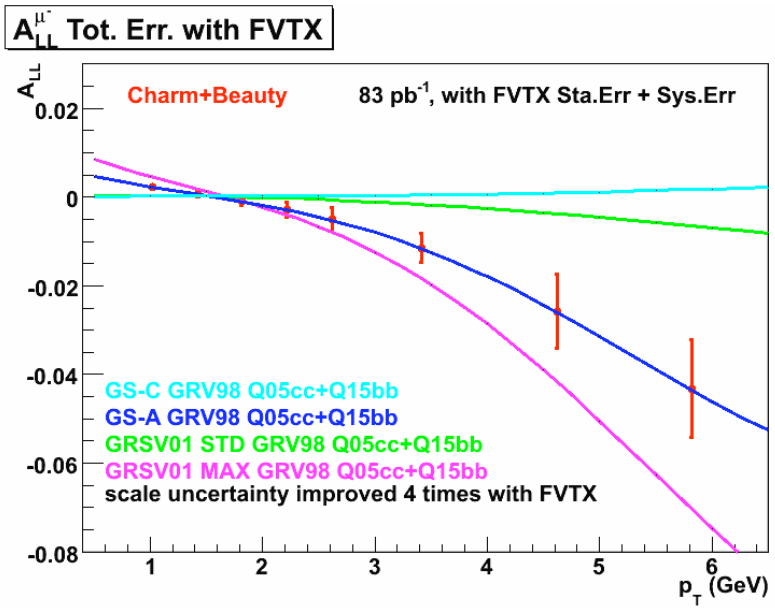

Figure 28 Heavy flavor A_{LL} measurement capabilities with the FVTX detector at 200 GeV for one year RHIC II running. The red points indicate the error bars we would obtain when the FVTX detector is used in the analysis with the muon arms. The theory curves are the predicted A_{LL} using GS-A, GS-C, GRSV-STD and GRSV-MAX for the polarized gluon distribution function.

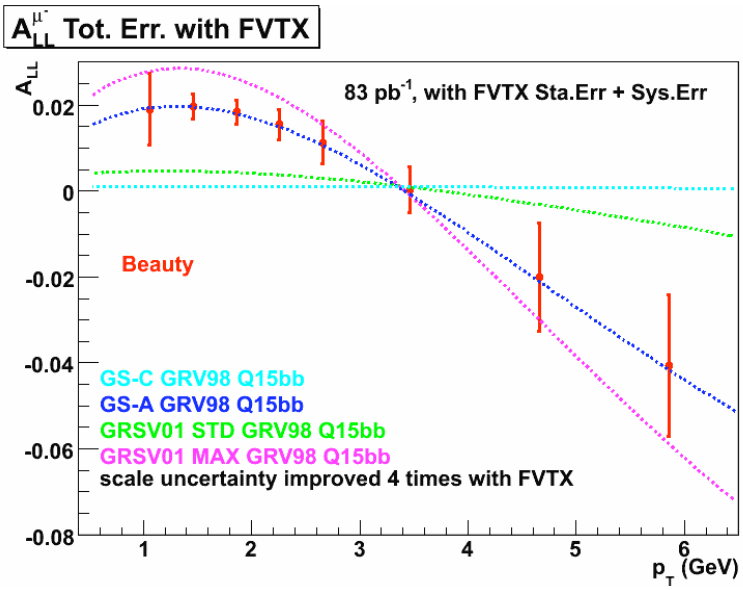

Figure 29 Beauty A_{LL} measurement capabilities with the FVTX detector. The theory curves are the predicted A_{LL} using GS-A, GS-C, GRSV-STD and GRSV-MAX for the polarized gluon distribution function. RHIC II luminosities are used.

2.7.3 Vector Meson Suppression and Debye Screening

The vector suppression pattern predicted for Au+Au collisions at RHIC, for charmonium and bottomonium mesons, is shown in Figure 30 versus the number of participants in the Au+Au collision. By adding the ψ' measurement to the current J/ψ measurements, plus upsilons as the RHIC luminosity increases, and χ_c from the nosecone calorimeter, we will get a clear picture of the suppression pattern versus the binding strength of the meson. From this, we will be able to say if the J/ψ is above or below the screening radius of the plasma (if the ψ' is highly suppressed, but the observed J/ψ yield misses only those J/ψs which arise from decays of ψ' and χ_c), and we will be able to see if the ψ' is suppression is consistent with large Debye screening. The addition of precision heavy flavor measurements via single muons will allow us to understand the potential contributions to charmonium production via regeneration. The J/ψ and ψ' are expected to have similar, but not exactly the same, contributions to their production from regeneration. If the ψ' is highly suppressed from screening, as is expected by theorists, then production via regeneration may be the primary production which is measured, especially in more central events. A centrality-dependent measurement of the ψ' compared to the J/ψ will help pull out the regeneration component as the falling ψ'/J/ψ ratio should plateau at the point where regeneration starts to become significant. A prediction of this behavior is shown in Figure 31, calculated by Grandchamp [8].

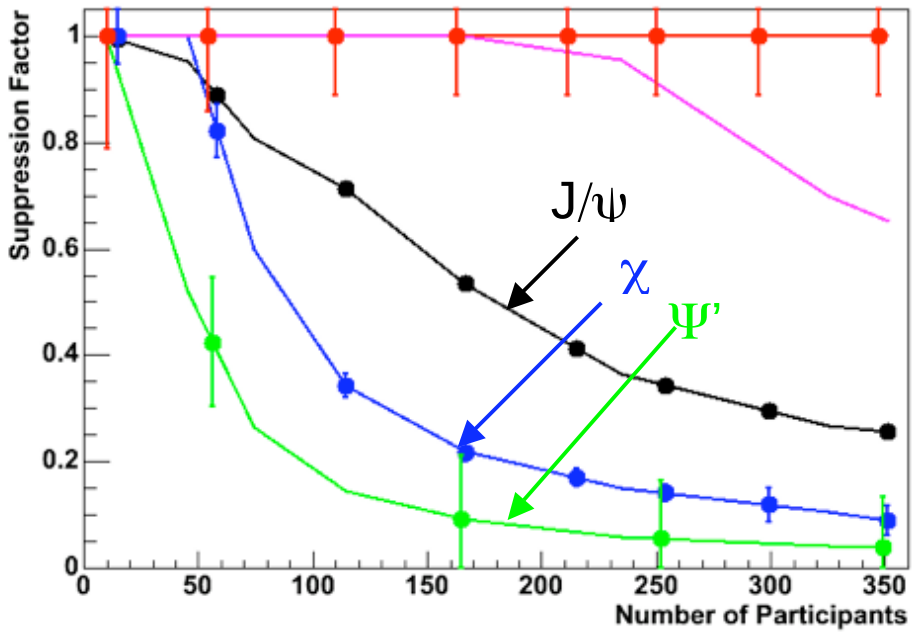

Figure 30 The suppression pattern we will be able to measure for the different heavy flavor vector mesons. The addition of the FVTX detector will give us access to the ψ' and the NCC will give access to the χ_c. Upsilons (red points) will be accessed with higher luminosities.

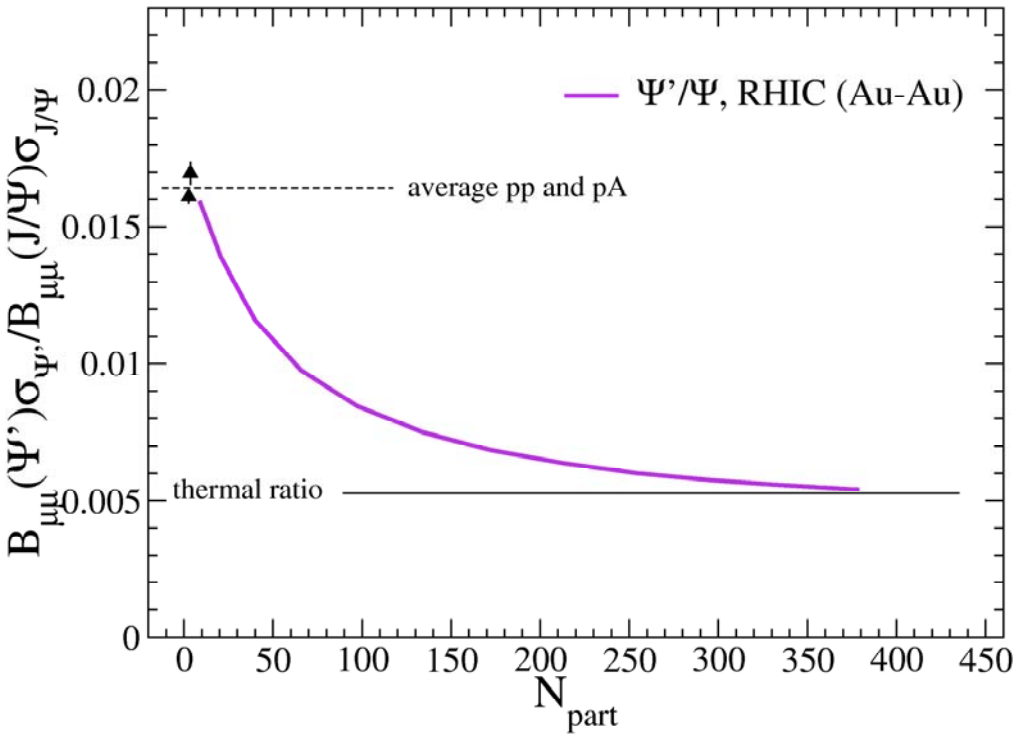

Figure 31 Predicted ψ'/J/ψ ratio in Au+Au collisions at RHIC. The ratio starts out at the p+p ratio, drops as suppression of ψ' is larger than suppression of J/ψ, and then plateaus as regeneration becomes a significant portion of the measured production.

3 Summary

We have presented in this report our simulated performance for heavy flavor R_{AA} measurements, ψ' measurements, and heavy flavor asymmetry measurements using the FVTX detector in conjunction with the muon arms. We have established that the detector performs well in either the p+p or Au+Au environment, is capable of providing significant suppression of backgrounds to single muon heavy flavor measurements, and can significantly improve the dimuon invariant mass resolution. For the first time we will have the capability of separating charm and beauty components in the forward rapidity region by making direct measurements of beauty and by statistically separating the two components with DCA cuts. With these added measurements, we will be able to provide critical measurements needed to understand the energy loss mechanisms in the QGP and we will be able to better understand the contributions of screening and regeneration to vector meson production. The rapidity coverage of the FVTX detector plus muon arms significantly expands the kinematic coverage of the PHENIX detector. This additional coverage will be needed to clearly separate cold nuclear matter effects and QGP effects on particle production. For the RHIC spin program we will add constraints to the polarized gluon distribution, via heavy flavor asymmetry measurements, in a critical x region which is not accessible by central rapidity detectors.

4 Appendix A – PDF Extraction from RHIC Data

To determine polarized parton distributions (PDFs), in particular, the gluon and anti-quark distributions, employing polarized proton collisions at high energy, is the most important goal of the RHIC spin program. The spin dependent inelastic p-p scattering cross sections factorize in to "products" of polarized parton distribution functions of protons and hard scattering cross sections describing spin dependent interactions of partons. The latter are calculable in QCD perturbation theory at next-to-leading (NLO). Knowing higher order corrections in perturbative expansion of partonic cross sections is generally very important because in hadronic scattering they can be often sizable, and because they also reduce the dependence of cross section on the choice of various unknown scales in the theory such as factorization, renormalization (scales). For most reactions relevant to the RHIC spin program NLO corrections to the cross sections are available, as such the foundation for determination of the polarized parton distribution at NLO already exists.

A complication common to A_{LL} probes of parton distributions in hadronic scattering is how to extract information about polarized PDFs in general from experimental data. We measure double spin asymmetries as functions of transverse momentum p_T of the measured final state particle, while the PDFs relevant to solving the nucleon spin puzzle need these to be in terms of partonic momentum fractions, *x*. For any measured data point in p_T, the gluon polarization is probed in a wide range in x_g, due to the convolutions inherent to the theoretical description of hard scattering cross sections. Therefore measured A_{LL} point vs. p_T has significant overlap with its neighbors in x_g. It is straightforward to use a model for $\Delta g(x_g)$ to predict $A_{LL}(p_T)$. However one cannot directly go the other way, i.e. to map points in p_T onto gluon polarization values vs. x_g. We emphasize two points here:

1. This is *not* unique to hadronic processes alone, semi-inclusive DIS measurements (high p_T di-hadron final state measurements in *l*-h scattering, for example) face the same issue.
2. It is often argued that measurement of final state correlations, (by going beyond inclusive measurements, such as p-p → γ-Jet, Jet-Jet), to determine the kinematics event by event, will solve this problem. This is *only* true if the parton distributions are being extracted at *leading order*, which should only be a first step towards determining the parton distributions, *not the ultimate goal*.

The ultimate goal of the RHIC spin program is to determine the polarized PDFs at highest order possible (presently NLO) in pertubative QCD using all RHIC spin data. This can best be achieved by analyzing the RHIC spin data and the polarized fixed target DIS data in a framework of a *global analysis*, similar to one that already exists in the form of CTEQ parton distribution functions for the unpolarized PDFs. The important advantage of such a global analysis is that it takes the measured experimental variables directly, rather than attempting to use derived or unmeasured variables in hadronic scattering such as *x*. Secondly, the uncertainties in the PDFs can be evaluated systematically taking in to account theoretical as well as experimental systematic uncertainties and their correlations. In order to do this over the widest possible kinematic range in x_g, in particular for the polarized gluon distribution, RHIC will have to be operated at different center of masses, both higher and lower than 200 GeV at which most of the operations have occurred so far. While this discussion is (apparently) only focused on the polarized gluon distribution, that was only for brevity. The situation, apart from the aspect of different center of mass operations, is identical in the case of determination of quark-anti-quark distributions with W physics measurements at RHIC. An effort to realize such a global analysis is now underway. In the next few years when the data from high luminosity, polarization and the detector upgrades for RHIC and the experiments get ready, so will be the analysis framework for the polarized PDFs. These together will enable the best possible extraction of polarized parton distribution functions.

[1] A. Adare *et al.* (PHENIX Collaboration), "Energy Loss and Flow of Heavy Quarks in Au+Au Collisions at $\sqrt{s_{NN}}$ = 200 GeV", nucl-ex/0611018 and submitted to Phys. Rev. Lett.
[2] I. Vitev, Phys. Lett. B **562**, 36 (2003).
[3] M. Djordjevic, M. Gyulassy nucl-th/0305062.
[4] M. Djordjevic, M. Gyulassy, Phys. Lett. **B560**, 37 (2003).
[5] S.S. Adler et al, hep-ex/0609032 "Measurement of Single Muons at Forward Rapidity in pp Collisions at sqrt(s)=200 GeV and Implications for Charm Production.
[6] M. Gyulassy, P. Levai, I. Vitev, Phys. Rev. Lett. **85**, 5535 (2000).
[7] I. Vitev, private communication.
[8] Loic Grandchamp-Desraux (SUNY, Stony Brook) . UMI-31-18472, 2003. 172pp.